

SDC Note SDC-92-361

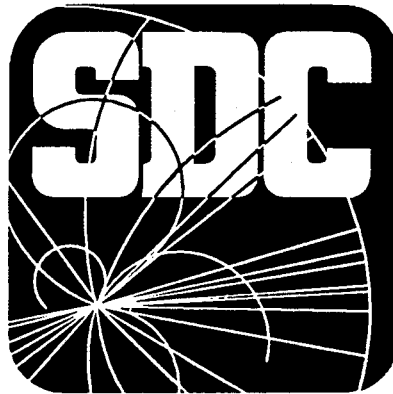
November 12, 1992

Neutron Currents in the SDC

*L. S. Waters, A. P. T. Palounek, H. G. Hughes,
H. Lichtenstein, R. E. Prael, and H. J. Ziock*
Los Alamos National Laboratory

It is clear that the SDC detector design must address the issues of radiation

SDC-92-361



SDC
SOLENOIDAL DETECTOR NOTES

NEUTRON CURRENTS IN THE SDC

November 12, 1992

*L.S. Waters, A.P.T. Palounek, H.G. Hughes,
H. Lichtenstein, R.E. Prael and H.J. Ziock*
Los Alamos National Laboratory

Neutron Currents in the SDC

*L. S. Waters, A. P. T. Palounek, H. G. Hughes,
H. Lichtenstein, R. E. Prael, and H. J. Ziock*
Los Alamos National Laboratory

It is clear that the SDC detector design must address the issues of radiation background and radiation damage to detector components. To that end, we have begun a comprehensive series of calculations to estimate the neutron backgrounds and radioactivation of the SDC detector. This note addresses neutron backgrounds in the SDC detector due to reactions stemming from primary minimum bias events. We will consider other aspects of the calculation series in future notes.

This note presents a first look at neutron backgrounds in the SDC detector. It is a scoping study to understand where the largest backgrounds and effects are. The next step will be to understand the sources of the neutrons and to minimize their impact. Some sources are obvious, while others are quite subtle. With the data in this note we can begin look for the major sources of neutrons. Such a search usually involves removing selected elements from the simulation and comparing the results. We will present the results of such comparisons in future notes.

We have simulated reactions in the entire SDC detector and several of the nearby beamline components using the Los Alamos High Energy Transport (LAHET) Monte Carlo code System [1, 2, 3, 4], as well as with the low energy neutron code MCNP [5]. Figure 1 shows the simulated detector and the surrounding hall. Figure 2 shows a detail of the transition region between the detector and the accelerator. The detector geometry and composition follow the SDC Parameters of July 1992 [6]. We have made no effort to simulate the detailed segmentation of the subdetectors; their composition represents an average of all materials within a given volume.

The high energy particle generation code DTUJET models the primary interactions at the SSC, simulating minimum bias events at 40 TeV. This study uses 250 minimum bias events.

We show calculated neutron currents through numerous surfaces at significant locations in the detector and surrounding areas in four separate plots: a) for neutron kinetic energy greater than 20 MeV; b) for neutron kinetic energies between 100 KeV

and 20 MeV; c) for neutron kinetic energies below 100 KeV; and d) for all neutrons. MCNP evaluated neutron cross sections are typically available up to 20 MeV. Neutron transport that is dominated by evaluated cross sections is thought to be more accurate than LAHET transport, which is a high energy transport Monte Carlo code and is used for energies MCNP cannot handle.

A neutron current is a count of neutrons that cross a given surface, regardless of angle. This is in contrast to the frequently presented flux, which can be estimated as the weighted track length per unit volume[†]. Although the neutron current is the total number of neutrons crossing a given surface, the currents shown in Figures 3-24 have been normalized to current/unit area for the surface segments on which they have been calculated. When the surface is at constant radius, we show the variation of the particle current with z (the longitudinal direction, with the interaction point at z = 0). Similarly, when the surface is at a constant longitudinal location, we show the variation of the current with radius. In all cases the units are number of neutrons × 10¹²/cm²/SSC year at a luminosity of 10³³. We have assumed 10⁷ seconds/SSC year.

† A particle flux is defined as $\Phi(r,E,t) = vN(r,E,t)$, where v is the particle speed and N is the particle density. The time-integrated flux is then

$$\int \Phi(r,E,t)dt = Wv \Delta t / V = WT_l / V,$$

where W is the particle weight, V is the cell volume, and T_l is the track length.

A particle current is defined as

$$\iiint J(r,E,t,\mu)dEdt\mu dA,$$

where $J(r,E,t,\mu)$ is the number of particles per second per unit energy per unit area per angle, r is the radius, E is the energy, t is time, $\mu = \cos(\theta)$, θ is the angle of the particle with respect to the normal to the plane of the cell, and A is the area.

References:

1. Richard E. Prael and Henry Lichtenstein, "User Guide to LCS: The LAHET Code System," LA-UR-89-3014, Los Alamos National Laboratory (September 1989).
2. R. E. Prael, "LAHET Benchmark Calculations of Differential Neutron Production Cross Sections for 113 MeV and 256 MeV Protons," Los Alamos National Laboratory Report number LA-UR-89-3347 (September 1989).
3. R. E. Prael, "LAHET Benchmark Calculations of Neutron Yields from Stopping-Length Targets for 113 MeV and 256 MeV Protons", Los Alamos National Laboratory report LA-UR-90-1620 (September 1989).
4. R. E. Prael, "LAHET Benchmark Calculations of Neutron Yields from 50 MeV Protons on Thick and Thin Targets," Los Alamos National Laboratory Report LA-CP-90-398 (August 1990).
5. J. F. Breismeister, *ed.*, "MCNP - A General Monte Carlo Code for Neutron and Photon Transport", LA-7396-M Rev. 2, Los Alamos National Laboratory (1986).
6. M. G. D. Gilchriese, *ed.*, "SDC Detector Parameters," Solenoidal Detector Collaboration Note SDT-000010, draft E (July, 1992).

Figure Captions:

Figure 1: A view of the SDC detector and its hall as modeled for this study.

Figure 2: A close-up of the region around $z=19\text{m}$. This shows the end of the quadrupole magnet, the magnet collimators, part of the forward calorimeter, and edges of several muon chambers.

Figure 3: Neutron currents at the first intermediate tracker layers (IT1) at $z=278\text{ cm}$. The tracker face extends from 34.7 cm to 98.4 cm, and is 168.9 cm from the front face of the endcap calorimeter.

Figure 4: Neutron currents between the endcap electromagnetic calorimeter and first hadronic endcap calorimeter, at $z=474.5\text{ cm}$. Note that the electromagnetic section of the endcap calorimeter is 1.1λ thick.

- Figure 5: Neutron currents between the two hadronic sections of the endcap calorimeter, at $z=570.5$ cm.
- Figure 6: Neutron currents at the outer edge of the phototubes just outside the endcap calorimeter, at $z=709.4$ cm. The apparent excess at low radii is due to the limited extent of the shield which causes a strong suppression of albedo neutrons from the forward calorimeter at larger radii.
- Figure 7: Neutron currents at the first forward muon chambers (FW1), at $z=753.7$ cm. The low value of the first radial bin is an artifact of the binning. The decrease with radius is roughly proportional to r^2 ; it is mostly an area effect. This implies the neutrons tend to come from the beamline.
- Figure 8: Neutron currents at the second plane of forward muon chambers (FW2), at $z=919.6$ cm.
- Figure 9: Neutron currents at the "fourth" plane of forward muon chambers (FW4), at $z=1385.6$ cm.
- Figure 10: Neutron currents at the fifth and final plane of forward muon chambers (FW5), at $z=1881.6$ cm. This plane sees a large neutron current reflected back from the collimator (higher energy neutrons) and from the concrete hall walls (lower energy and thermal neutrons).
- Figure 11: Neutron currents within the first quadrupole magnet, at $z=2061.43$ cm.
- Figure 12: Neutron currents within a quadrupole magnet, at $z=5498.89$ cm. This is the junction between the SDC hall and the accelerator tunnel.
- Figure 13: Neutron currents at the location of the first cylindrical layer of the silicon tracker, at $r=9$ cm. The barrel tracker planes extend to ± 30 cm in z , though we show currents along the entire silicon tracking length of ± 258 cm.
- Figure 14: Neutron currents at the location of the last layer of the barrel silicon tracker, at $r=36$ cm. The barrel tracker planes extend to ± 30 cm in z , though we show currents along the entire silicon tracking length of ± 258 cm.

- Figure 15: Neutron currents between the electromagnetic and first hadronic sections of the barrel calorimeter, at $r=239$ cm. The barrel electromagnetic section is 0.85λ thick, at 90° , while the coil is 0.25λ thick there.
- Figure 16: Neutron currents between the two hadronic sections of the barrel calorimeter, at $r=323$ cm. The first hadronic barrel section adds an additional 4.14λ at 90° .
- Figure 17: Neutron currents at the outside of the barrel calorimeter phototubes, at $r=463.1$ cm.
- Figure 18: Neutron currents through a cylinder at $r=575.6$ cm, the location of the first planes of the barrel muon chambers (BW1). The muon chambers see albedo neutrons from the forward calorimeter and from the collimator. Those backslash neutrons are attenuated by the forward and barrel toroids.
- Figure 19: Neutron currents through a cylinder at $r=848$ cm, the location of the second planes of the barrel muon chambers (BW2).
- Figure 20: Neutron currents through a cylinder at $r=990.1$ cm, the location of the third planes of the barrel muon chambers (BW3).
- Figure 21: Neutron currents of neutrons moving back toward the detector from the front face of the forward calorimeter, at $z=1274.6$ cm.
- Figure 22: Neutron currents for neutrons emitted into the SDC hall or into the accelerator tunnel from the quadrupole cryostat as a function of z . The peaks in the high energy spectrum and the dips in the low energy spectrum correspond to the drift spaces between the magnets.
- Figure 23: The transmitted neutron currents for the detector hall wall at $z=55$ m, as a function of x -position and y -position in cm. These plots show the neutrons transmitted by the wall, that is, neutrons that continue traveling away from the detector.

Figure 24. The reflected neutron currents for the detector hall wall at $z=55$ m, as a function of x -position and y -position in cm. These plots show the neutrons reflected by the wall, that is, neutrons that travel toward the detector. Note the rough equality between the currents shown in Figures 23 and 24, which indicates that most of the transmitted neutrons are eventually reflected.

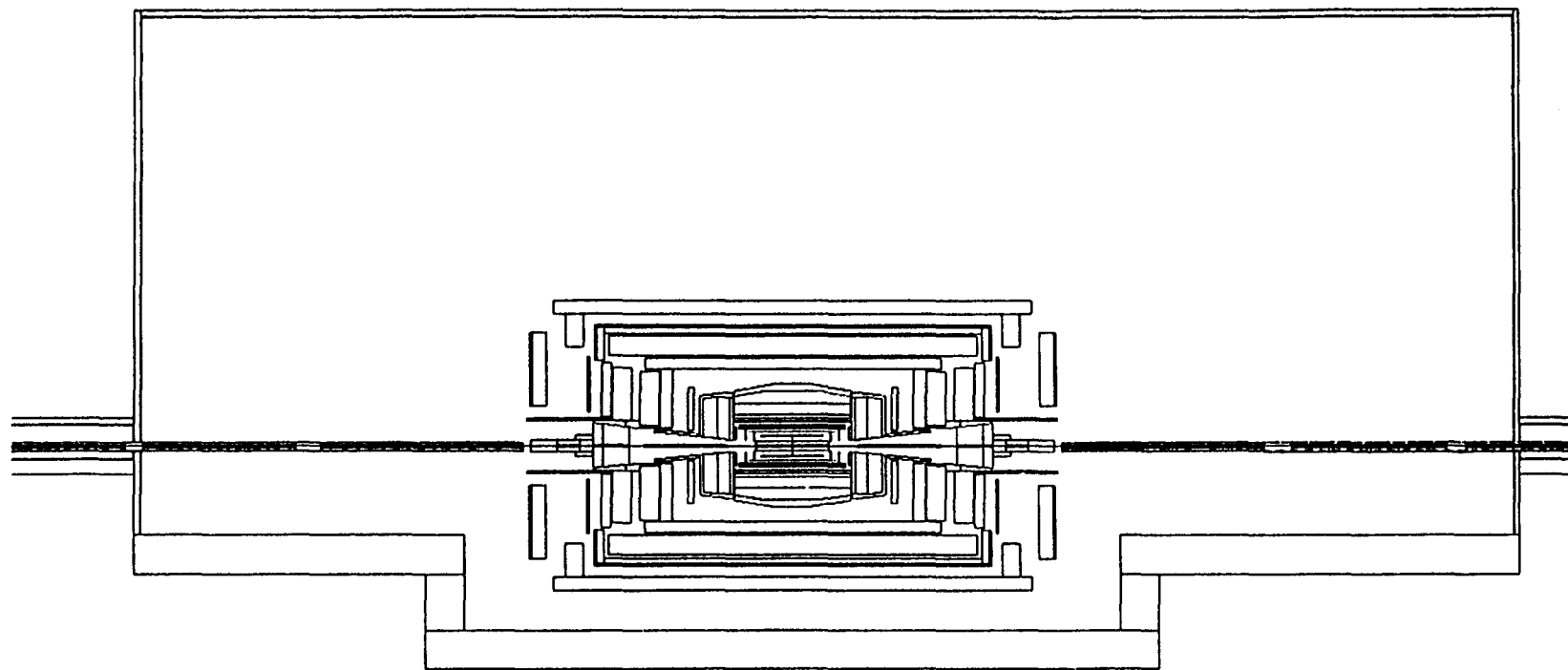


Figure 1: A view of the SDC detector and its hall as modeled for this study.

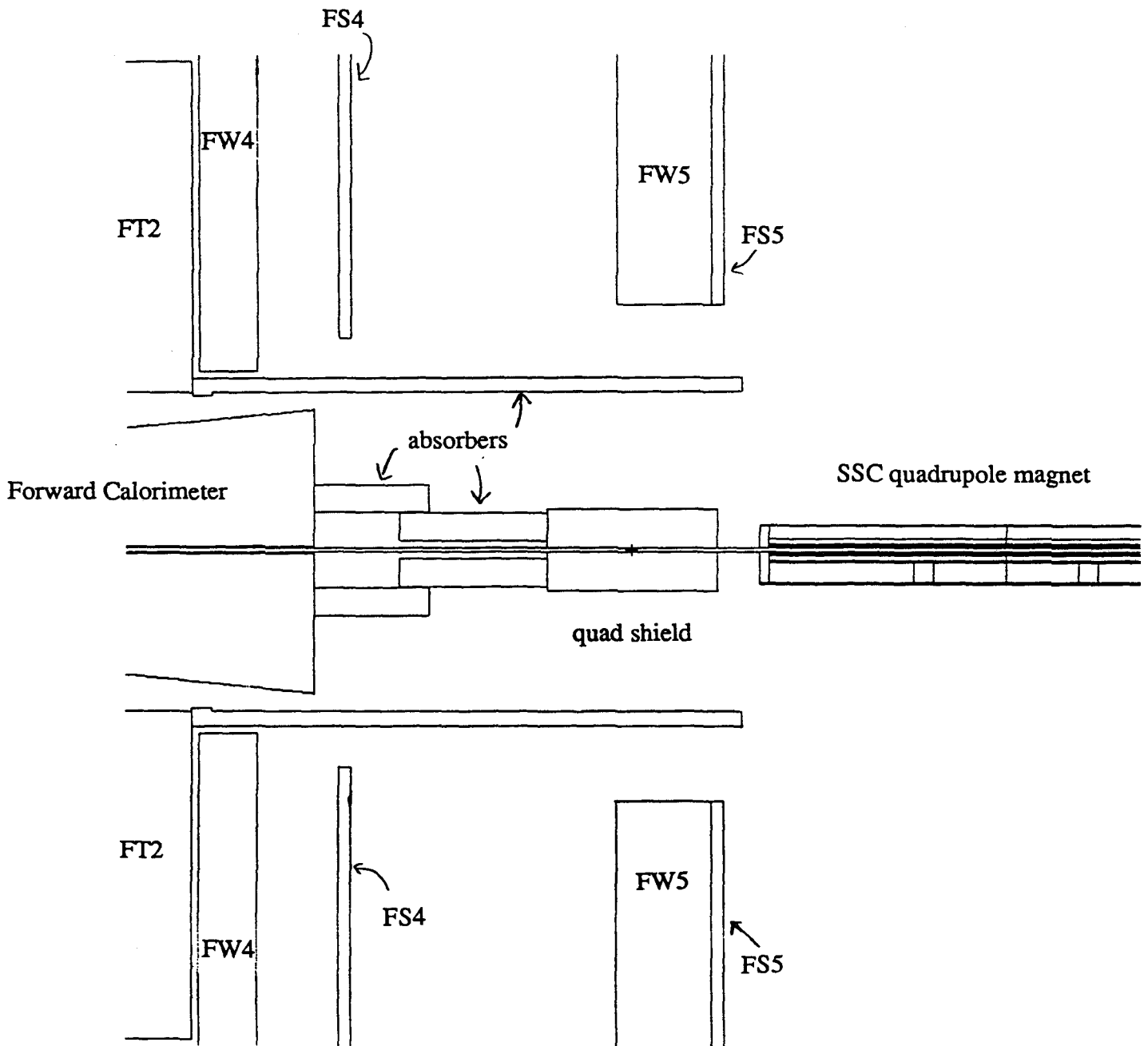


Figure 2: A close-up of the region around $z=19\text{m}$. This shows the end of the quadrupole magnet, the magnet collimators, part of the forward calorimeter, and edges of several muon chambers.

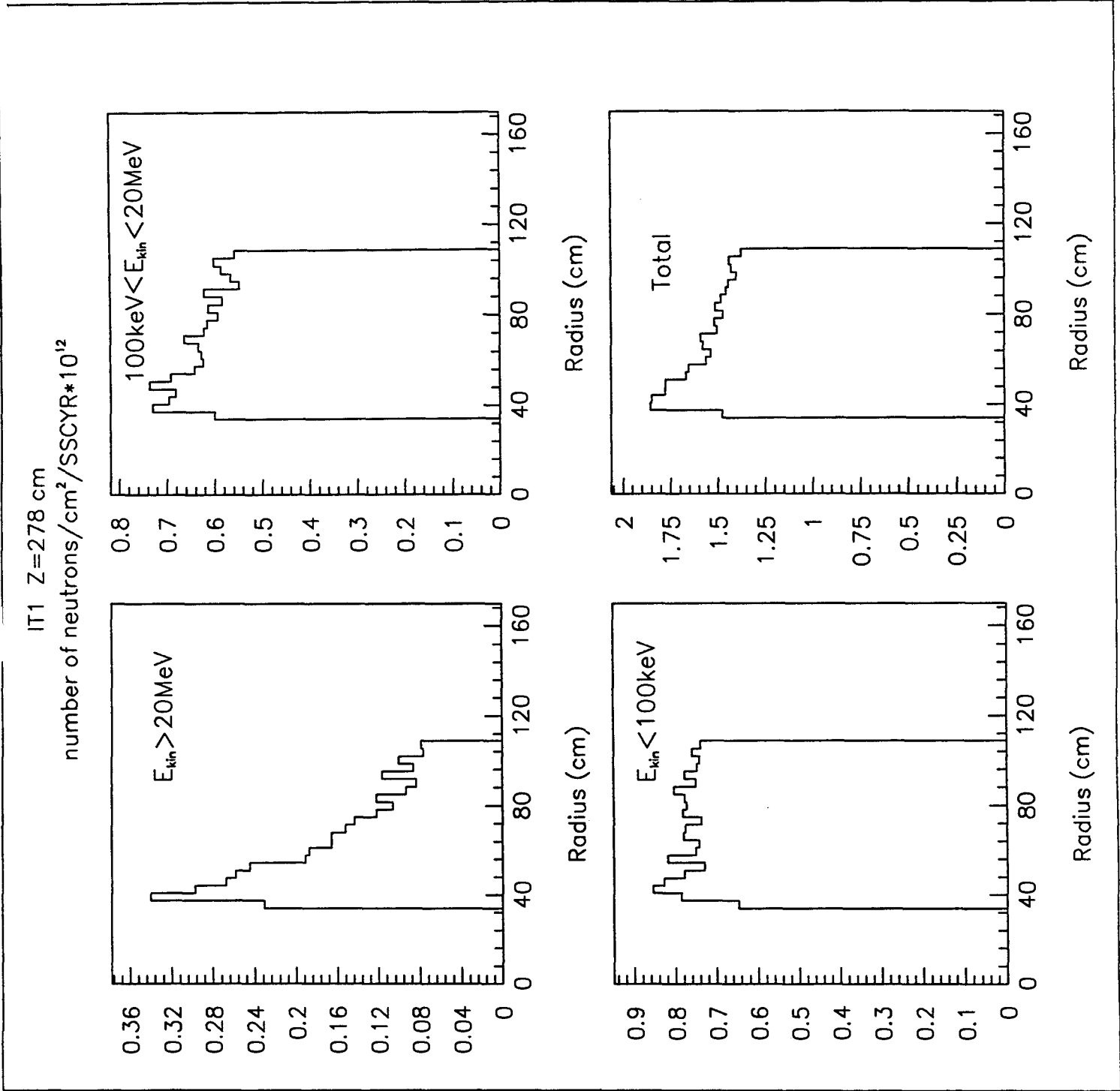
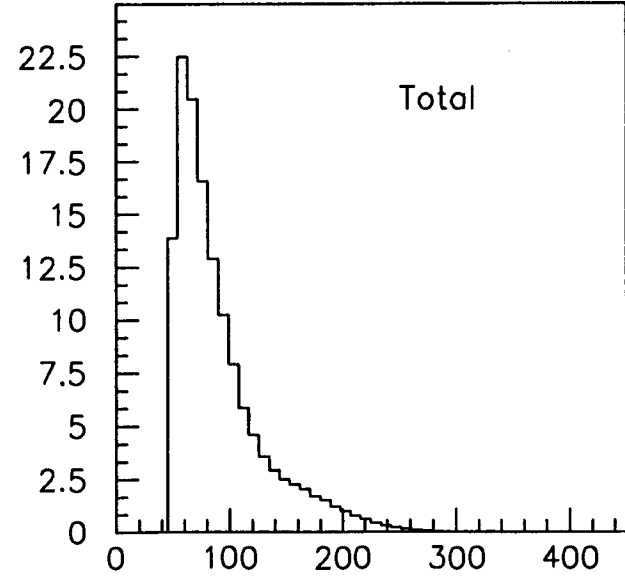
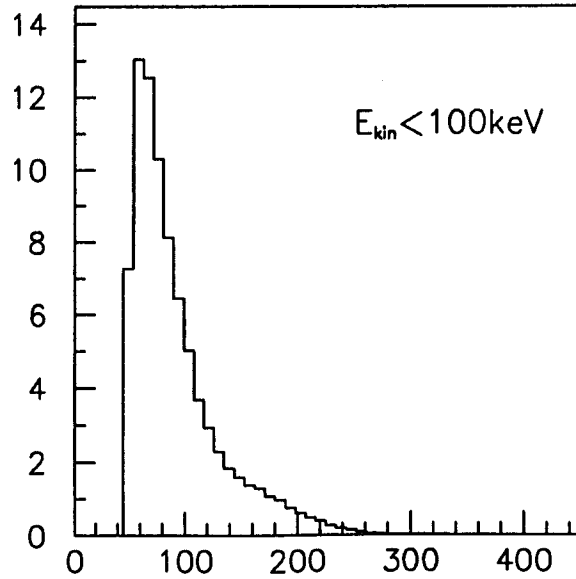
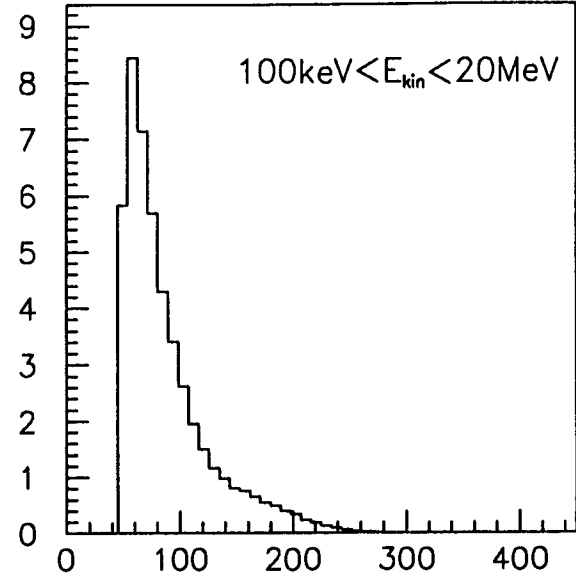
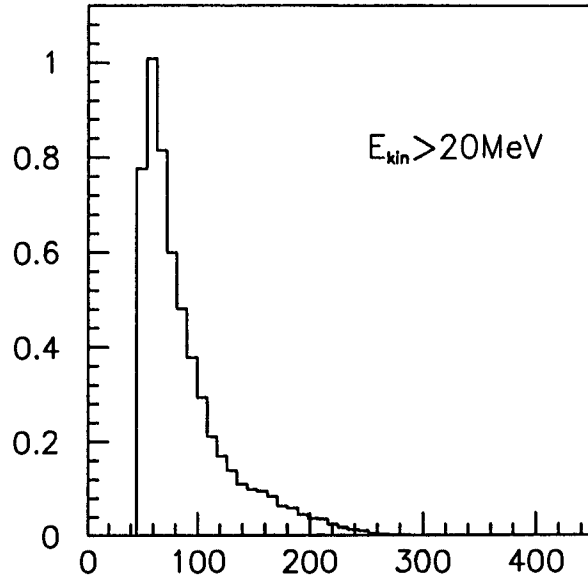


Figure 3: Neutron currents at the first intermediate tracker layers (IT1) at z=278 cm. The tracker face extends from 34.7 cm to 98.4 cm, and is 168.9 cm from the front face of the endcap calorimeter.

Endcap EM to HAD1 Z=474.5 cm
number of neutrons/cm²/SSCYR*10¹²



Radius (cm)

Radius (cm)

Radius (cm)

Radius (cm)

Figure 4: Neutron currents between the endcap electromagnetic calorimeter and first hadronic endcap calorimeter, at $z=474.5 \text{ cm}$. Note that the electromagnetic section of the endcap calorimeter is 1.1λ thick.

HAD1 TO HAD2 Z=570.5 cm
number of neutrons/cm²/SSCYR*10¹²

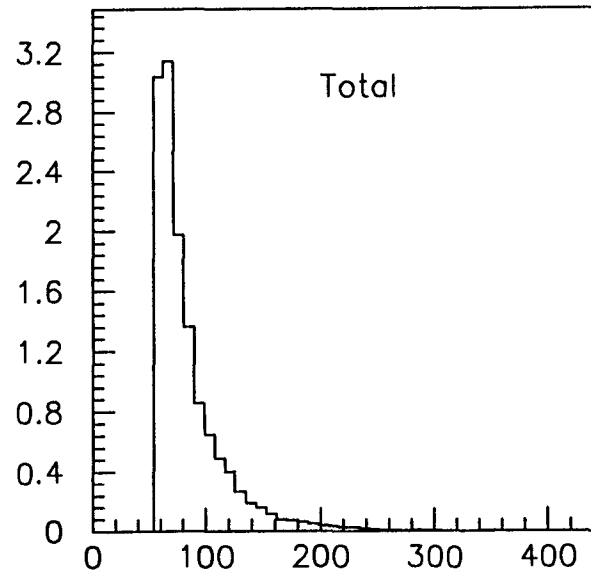
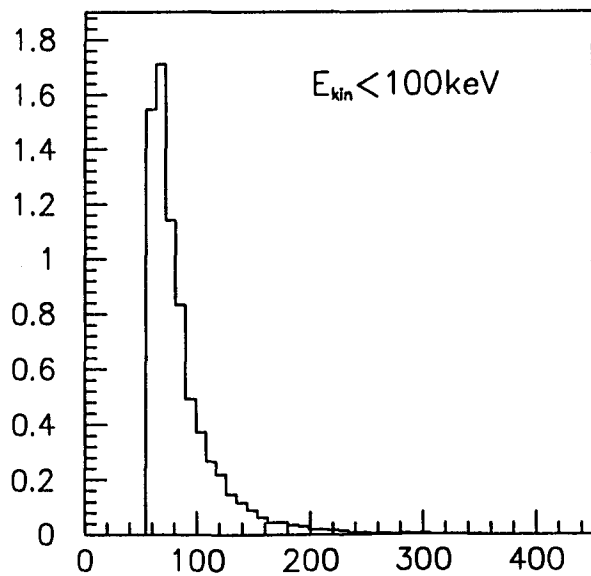
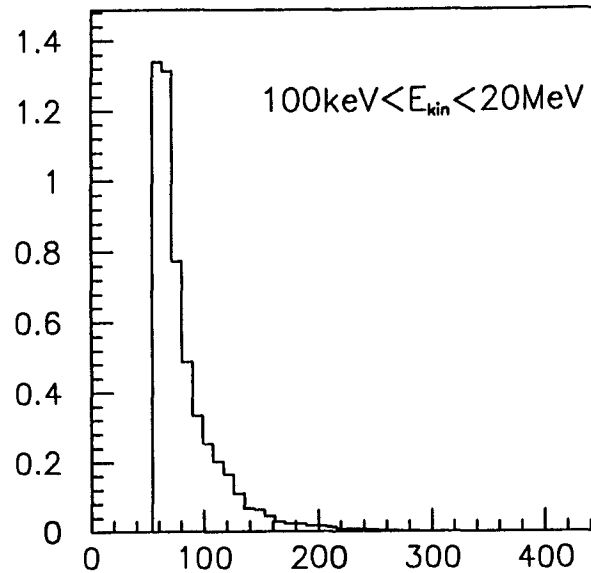
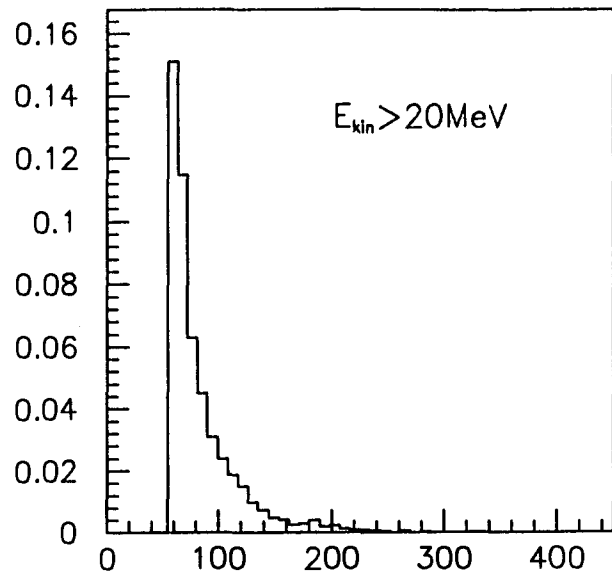


Figure 5: Neutron currents between the two hadronic sections of the endcap calorimeter, at $z=570.5 \text{ cm}$.

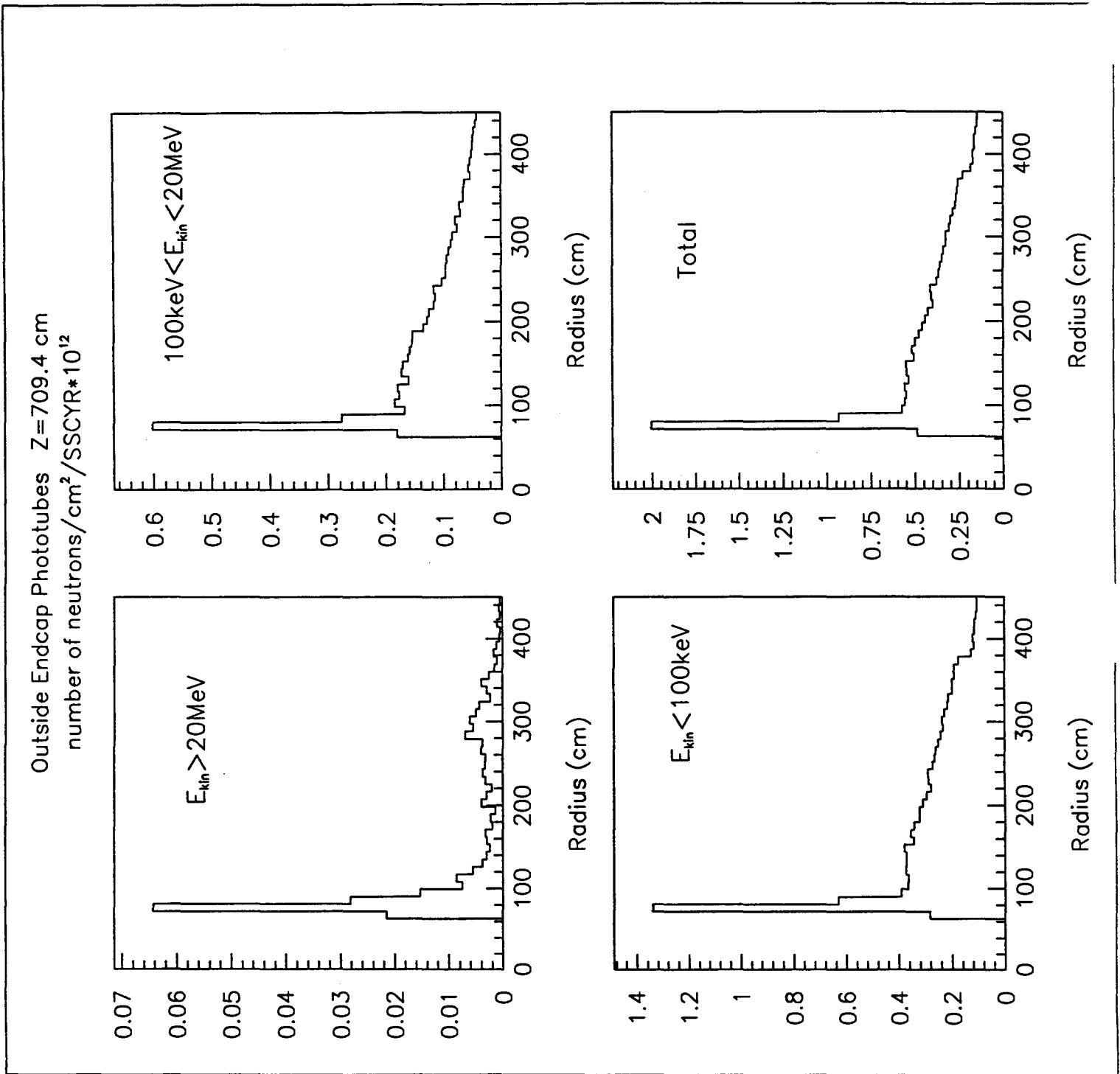


Figure 6: Neutron currents at the outer edge of the phototubes just outside the endcap calorimeter, at $z=709.4$ cm. The apparent excess at low radii is due to the limited extent of the shield which causes a strong suppression of albedo neutrons from the forward calorimeter at larger radii.

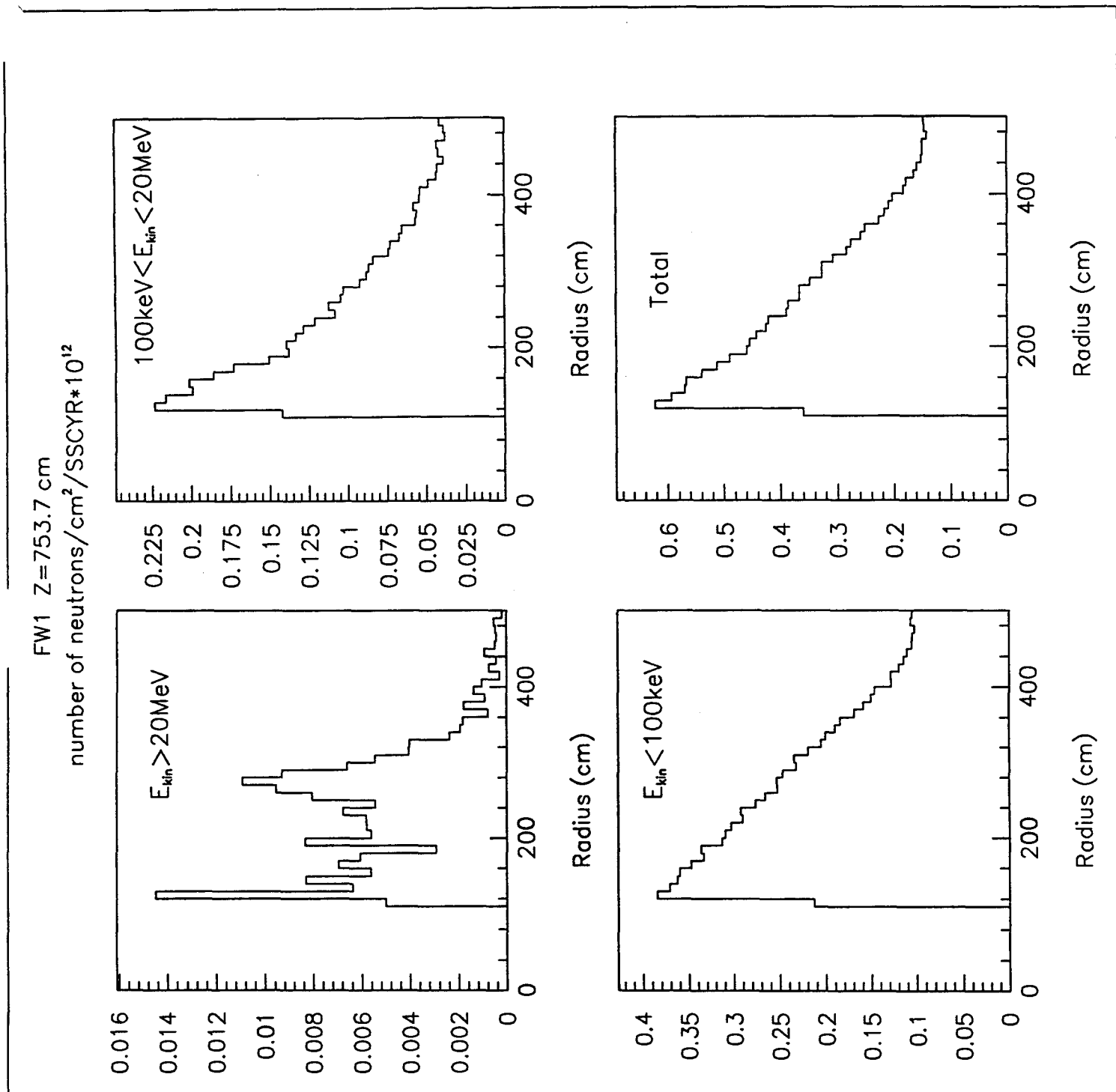


Figure 7: Neutron currents at the first forward muon chambers (FW1), at $z=753.7$ cm. The low value of the first radial bin is an artifact of the binning. The decrease with radius is roughly proportional to r^2 ; it is mostly an area effect. This implies the neutrons tend to come from the beamline.

FW2 Z=919.6 cm
number of neutrons/cm²/SSCYR*10¹²

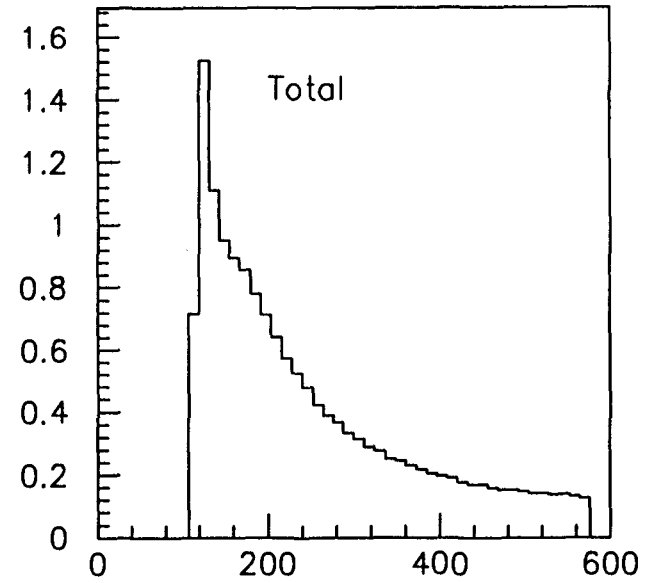
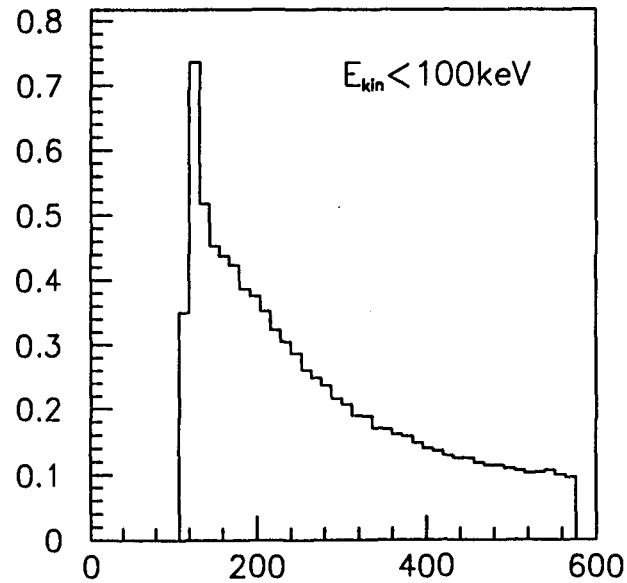
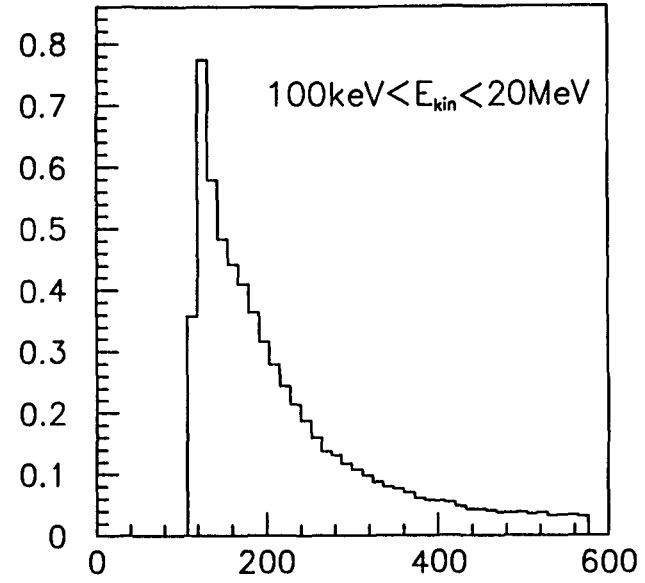
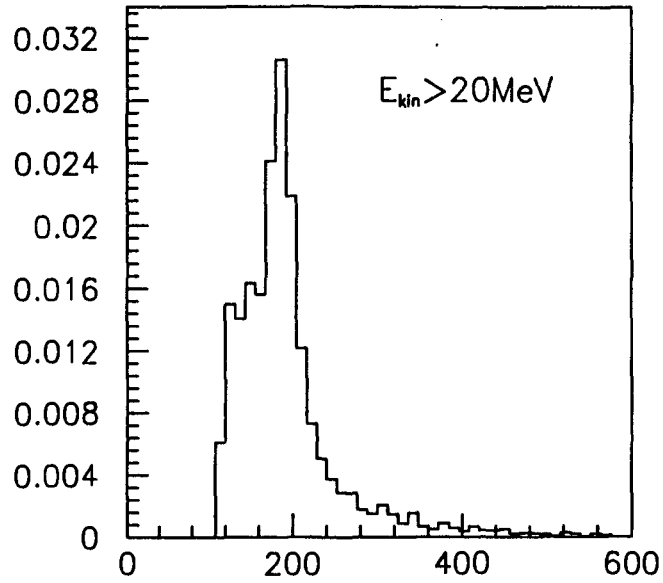


Figure 8: Neutron currents at the second plane of forward muon chambers (FW2), at $z = 919.6 \text{ cm}$.

FW4 Z=1385.6 cm
number of neutrons/cm²/SSCYR*10¹²

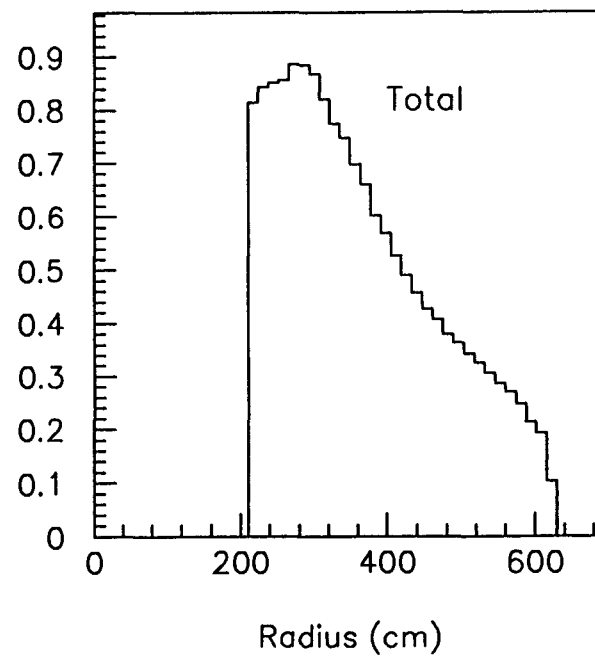
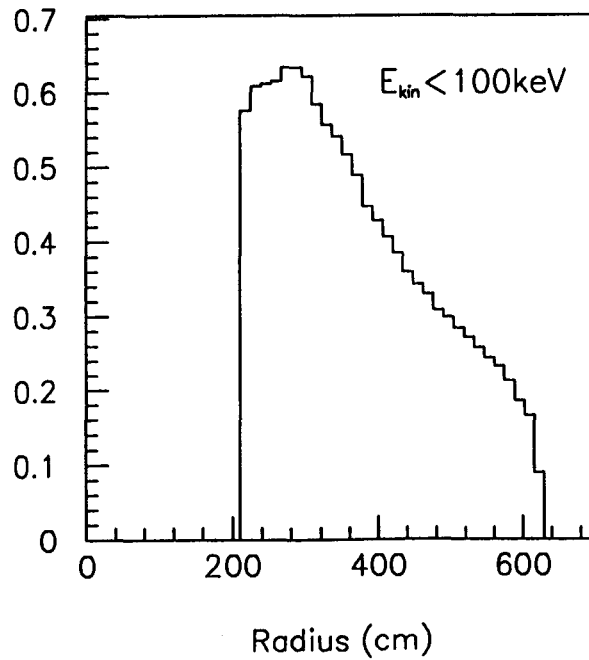
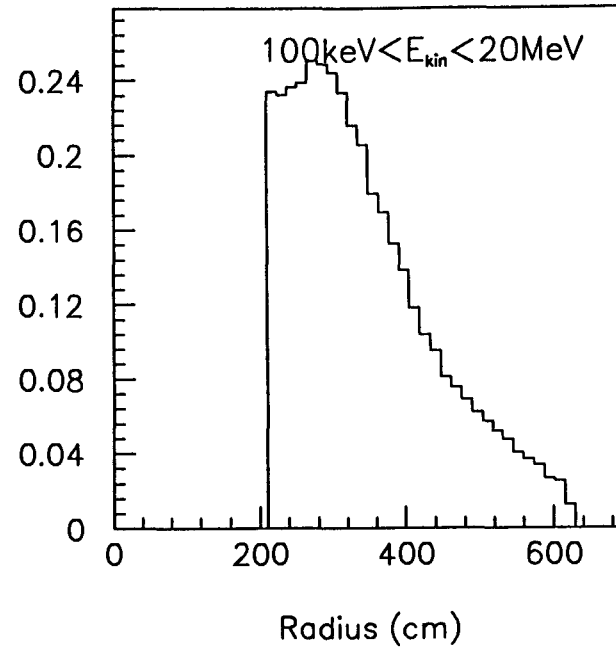
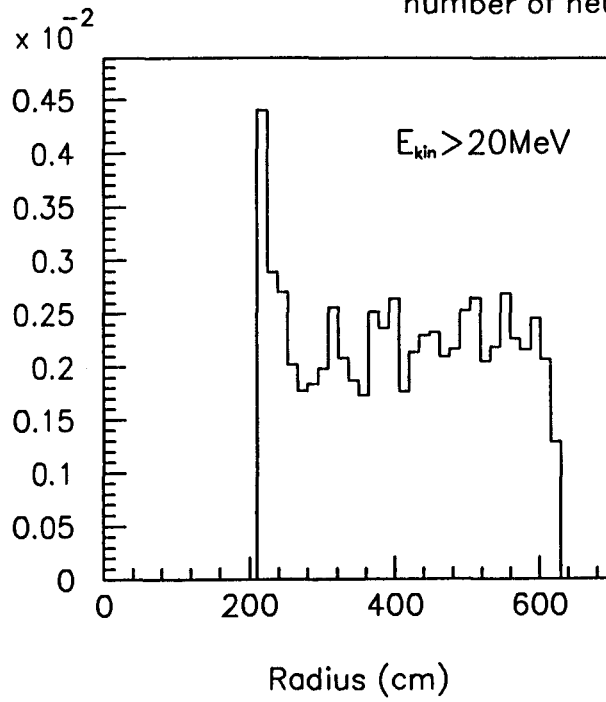


Figure 9: Neutron currents at the "fourth" plane of forward muon chambers (FW4), at $z=1385.6 \text{ cm}$.

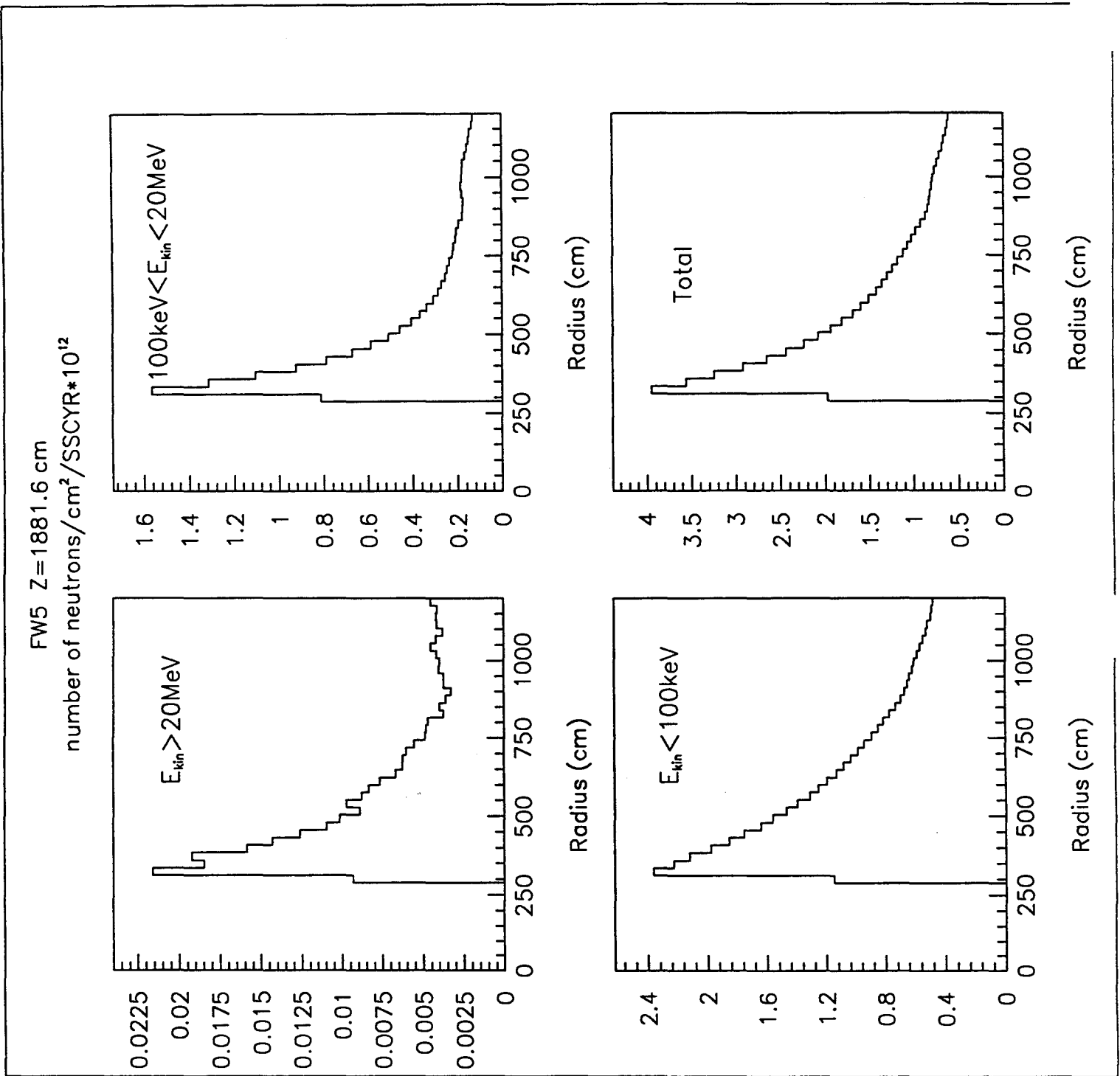


Figure 10: Neutron currents at the fifth and final plane of forward muon chambers (FW5), at $z=1881.6$ cm. This plane sees a large neutron current reflected back from the collimator (higher energy neutrons) and from the concrete hall walls (lower energy and thermal neutrons).

Magnet Z=2061.43 cm
number of neutrons/cm²/SSCYR*10¹²

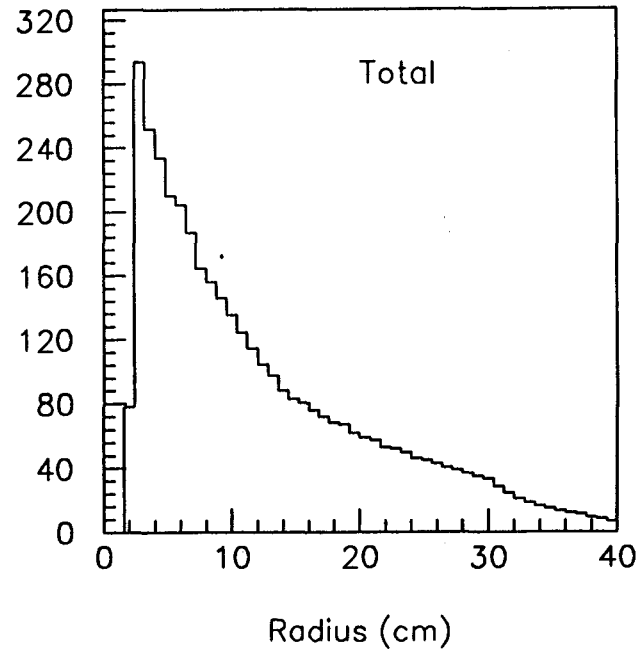
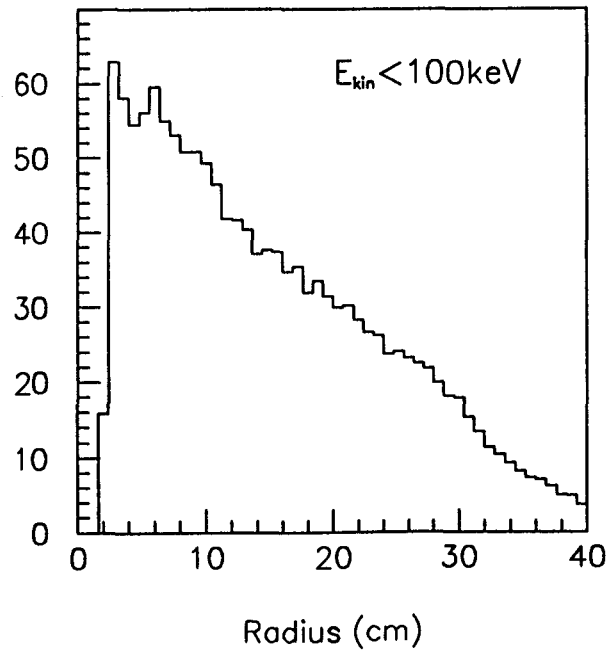
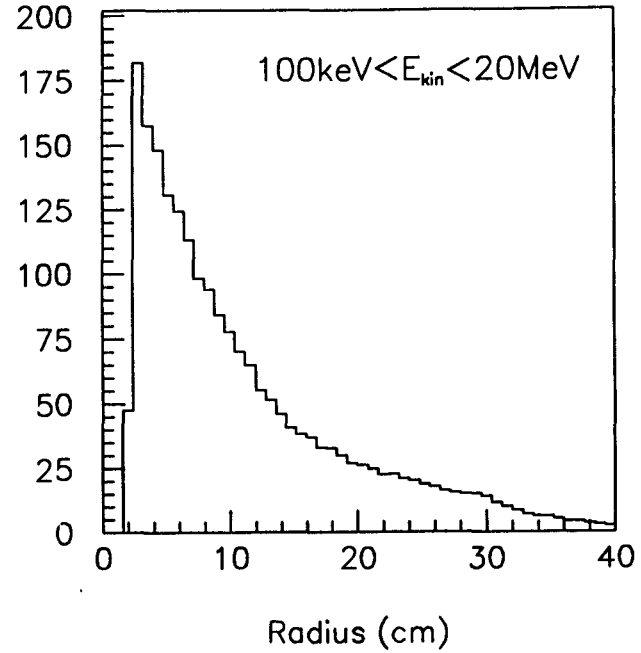
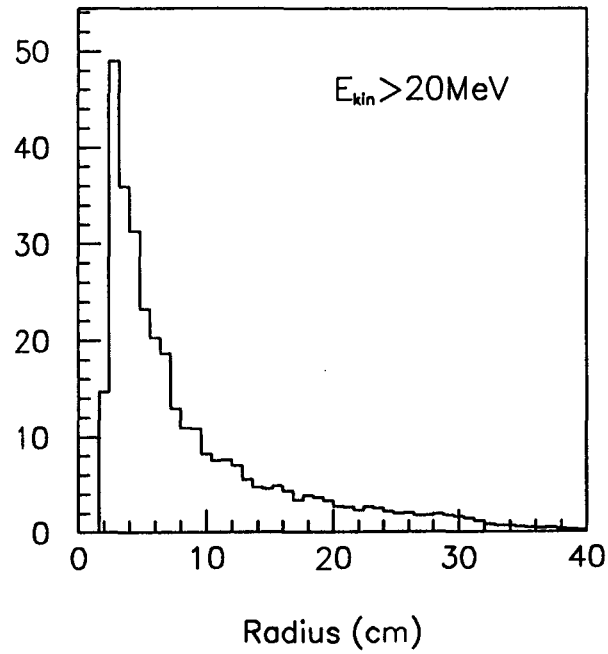


Figure 11: Neutron currents within the first quadrupole magnet, at z=2061.43 cm.

Magnet Z=5498.8875 cm
number of neutrons/cm²/SSCYR*10¹²

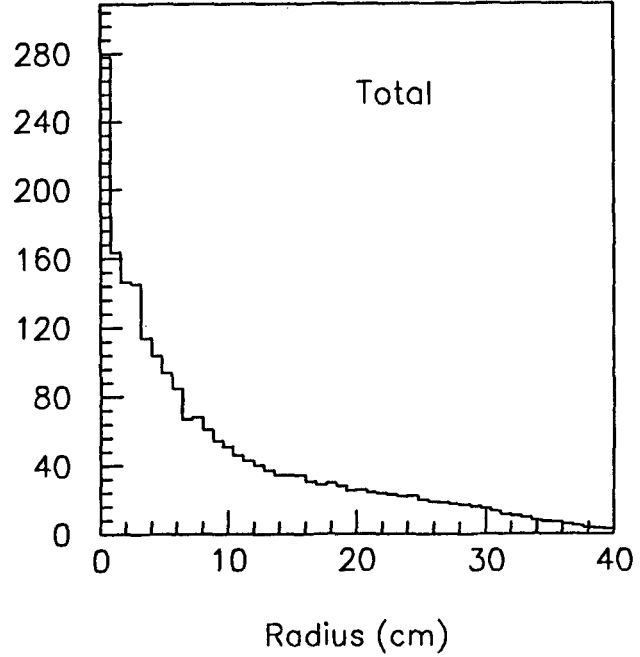
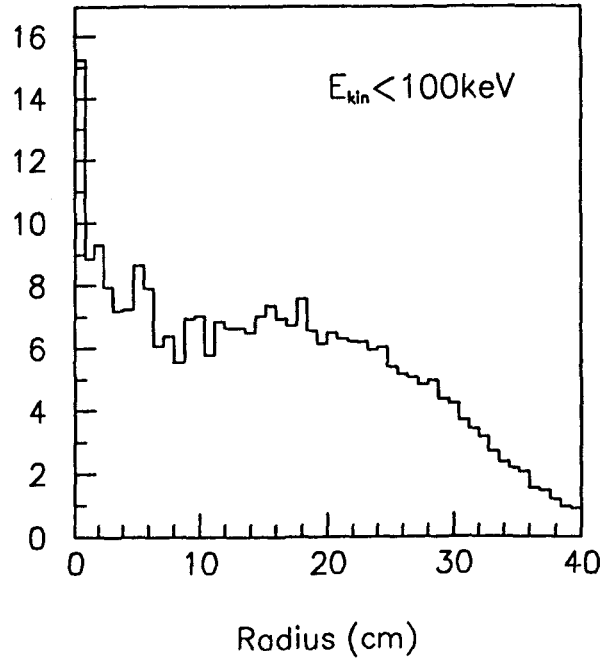
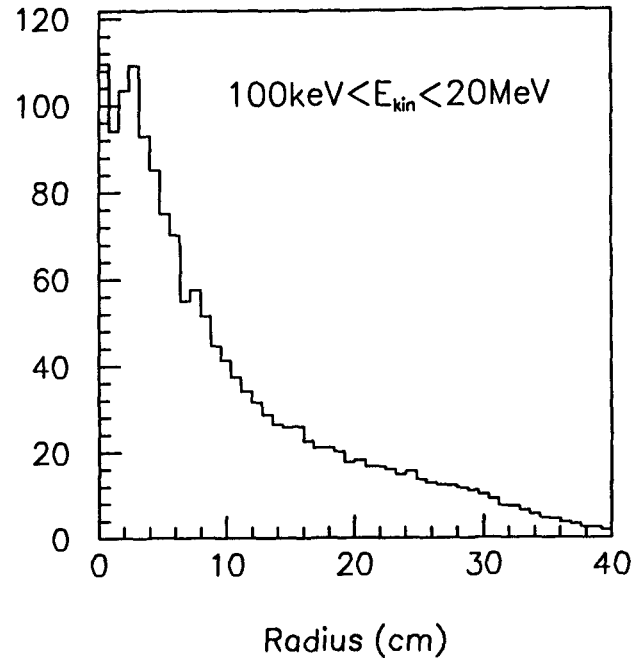
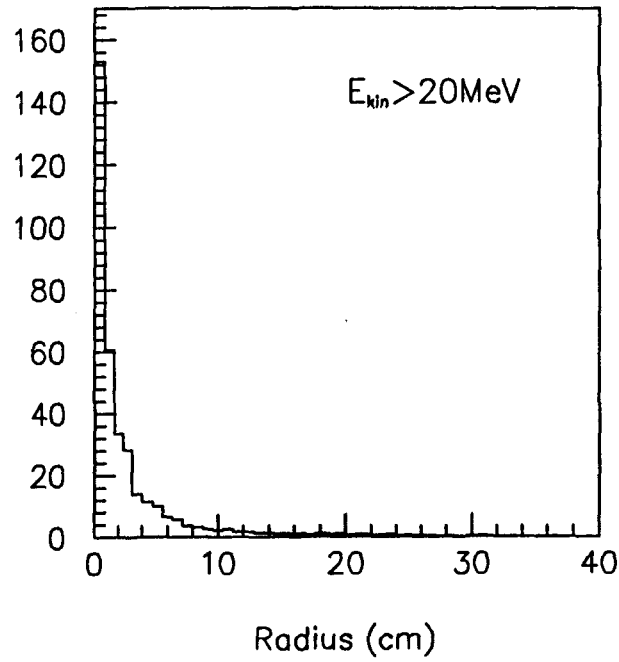


Figure 12: Neutron currents within a quadrupole magnet, at $z=5498.89 \text{ cm}$. This is the junction between the SDC hall and the accelerator tunnel.

Central Tracker Region Radius = 9 cm
number of neutrons/cm²/SSCYR*10¹²

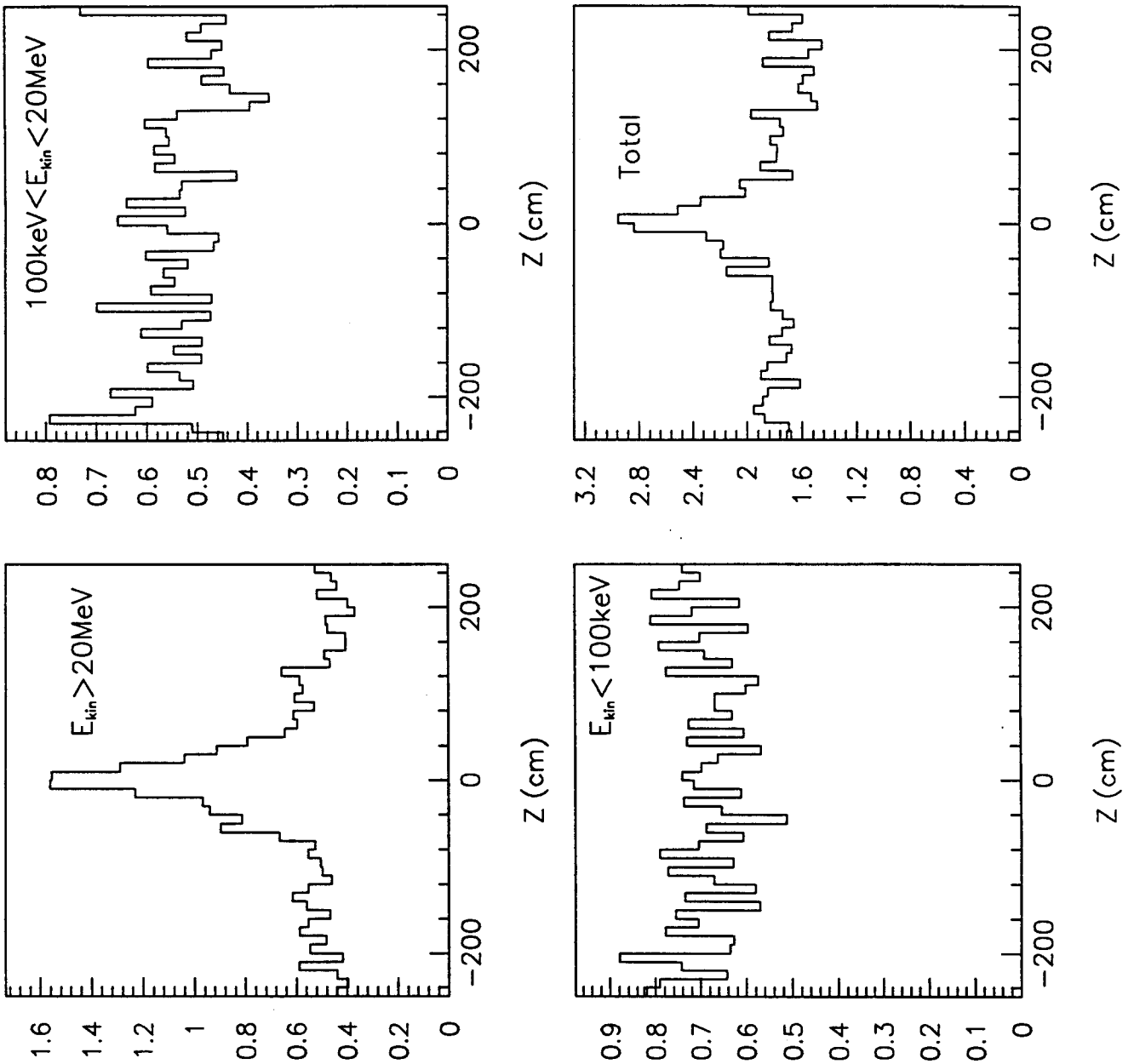


Figure 13: Neutron currents at the location of the first cylindrical layer of the silicon tracker, at $r=9$ cm. The barrel tracker planes extend to ± 30 cm in z , though we show currents for the entire silicon tracking length of ± 258 cm.

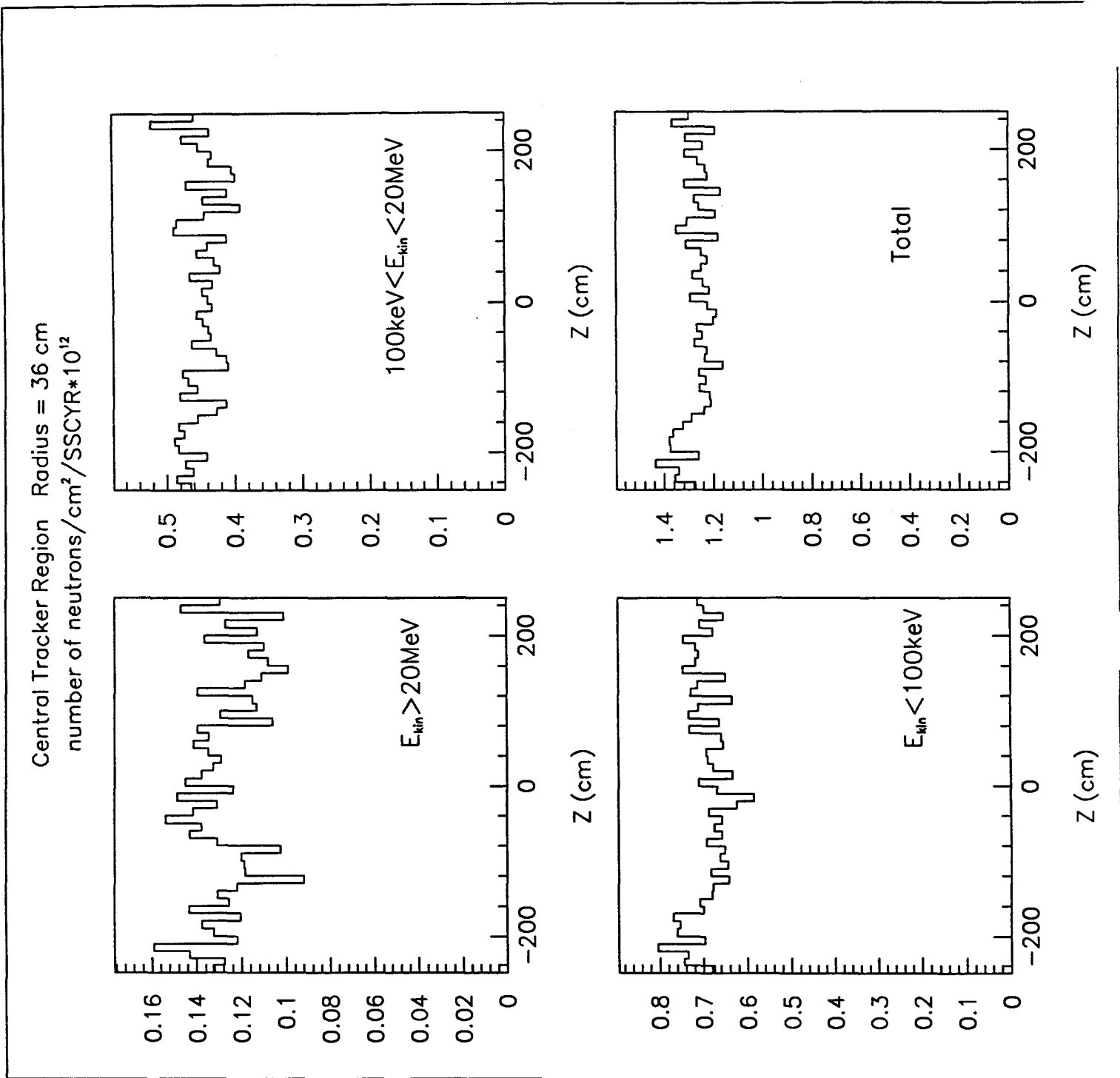


Figure 14: Neutron currents at the location of the last layer of the barrel silicon tracker, at $r=36$ cm. The barrel tracker planes extend to ± 30 cm in z , though we show currents for the entire silicon tracking length of ± 258 cm.

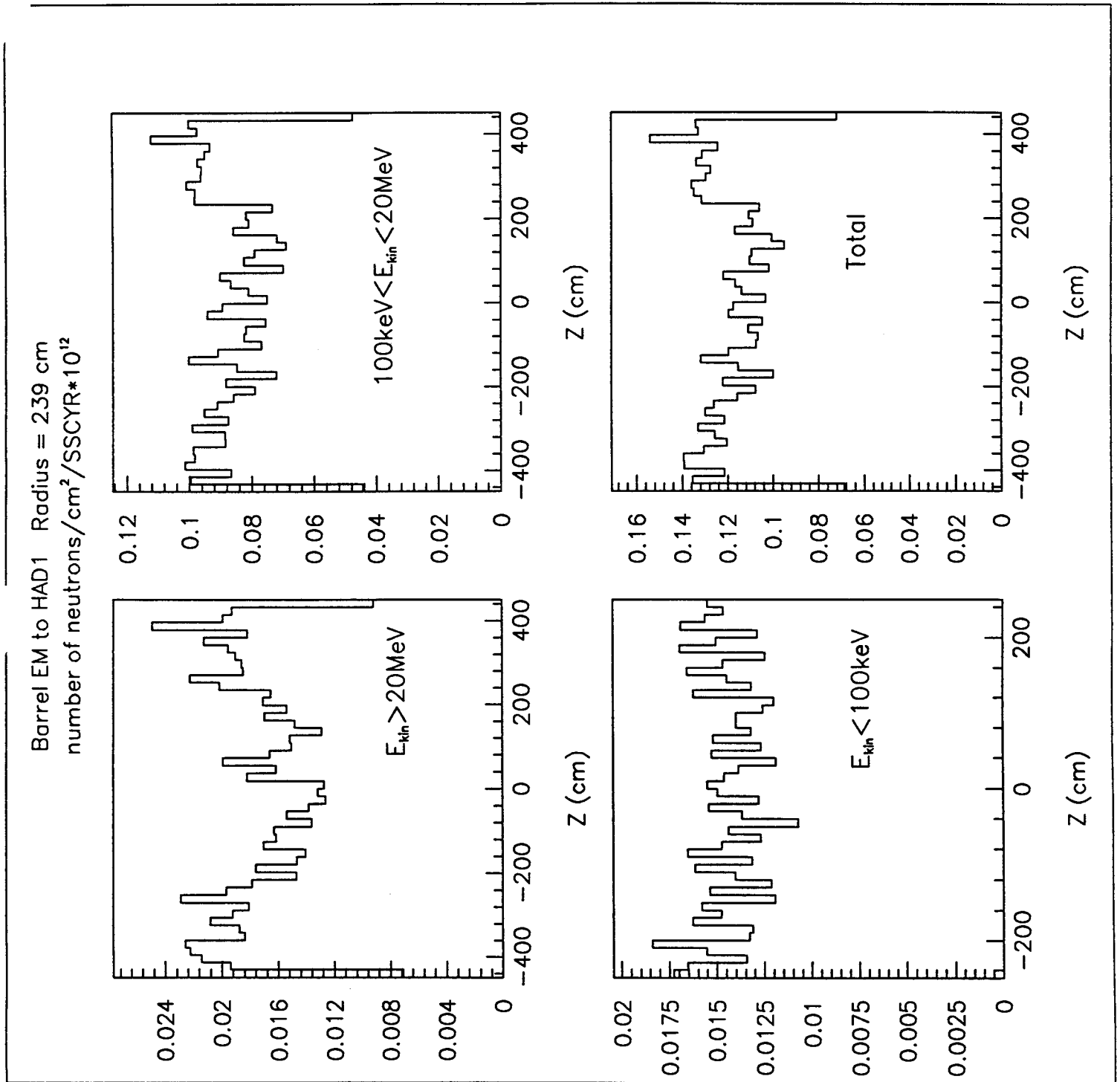


Figure 15: Neutron currents between the electromagnetic and first hadronic sections of the barrel calorimeter, at $r=239$ cm. The barrel electromagnetic section is 0.85λ thick, at 90° , while the coil is 0.25λ thick there.

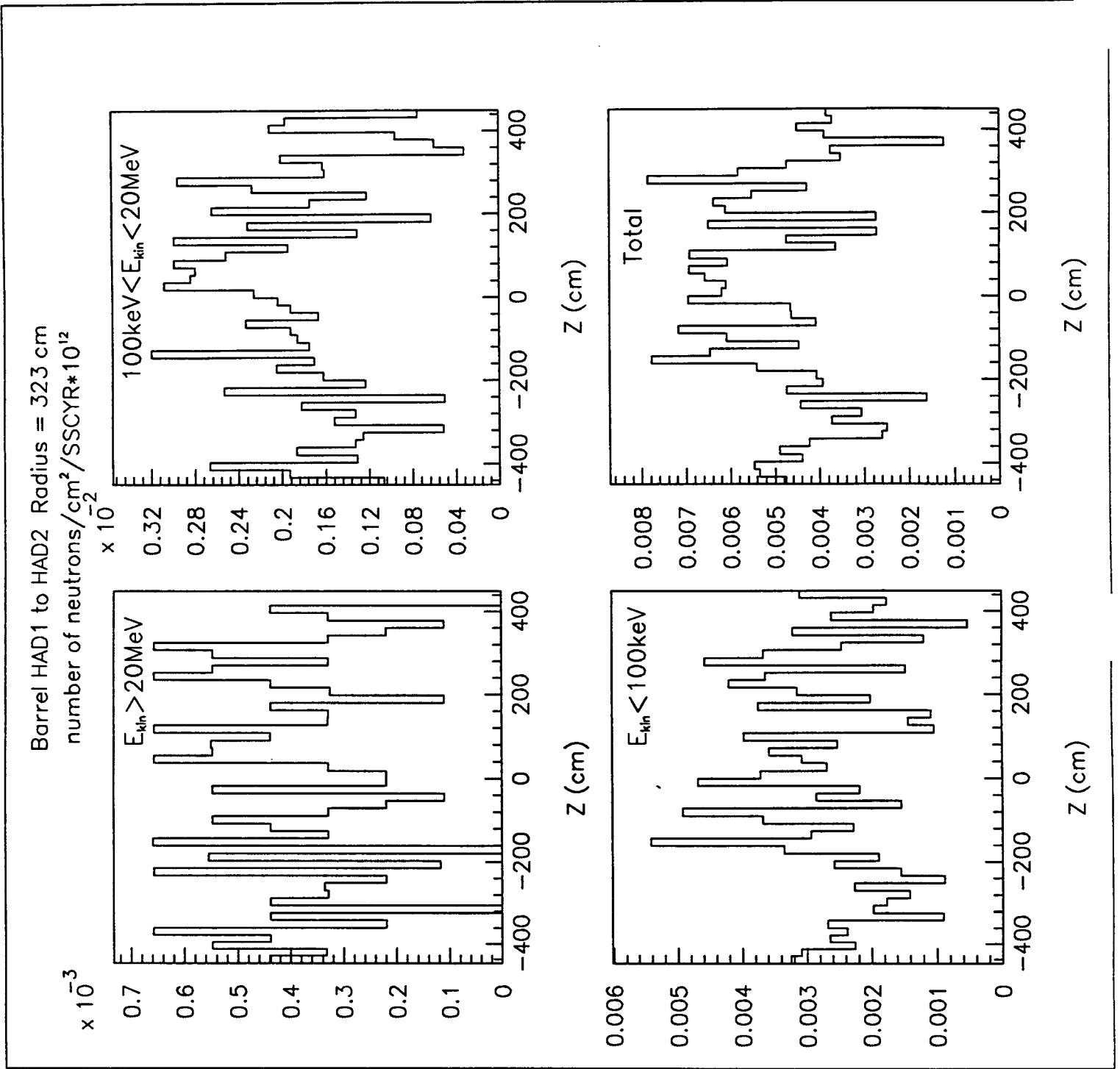


Figure 16: Neutron currents between the two hadronic sections of the barrel calorimeter, at $r=323$ cm. The first hadronic barrel section adds an additional 4.14λ at 90° .

Outside Barrel Phototubes Radius=463.1 cm
number of neutrons/cm²/SSCYR*10¹²

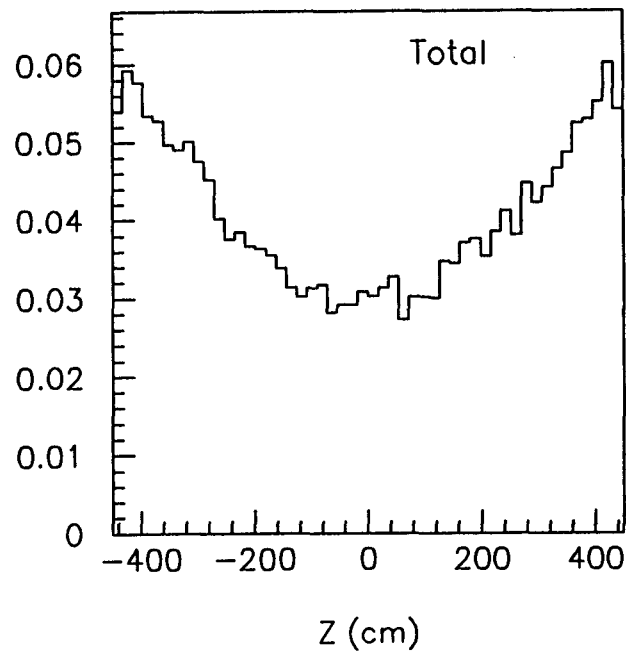
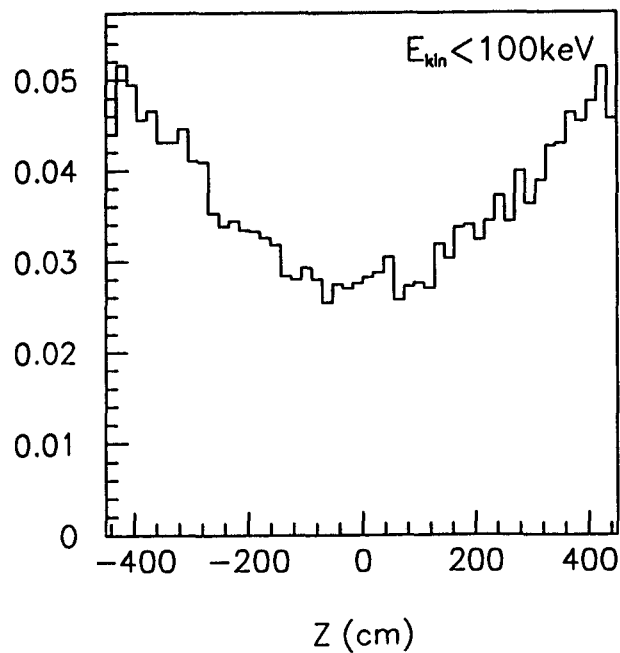
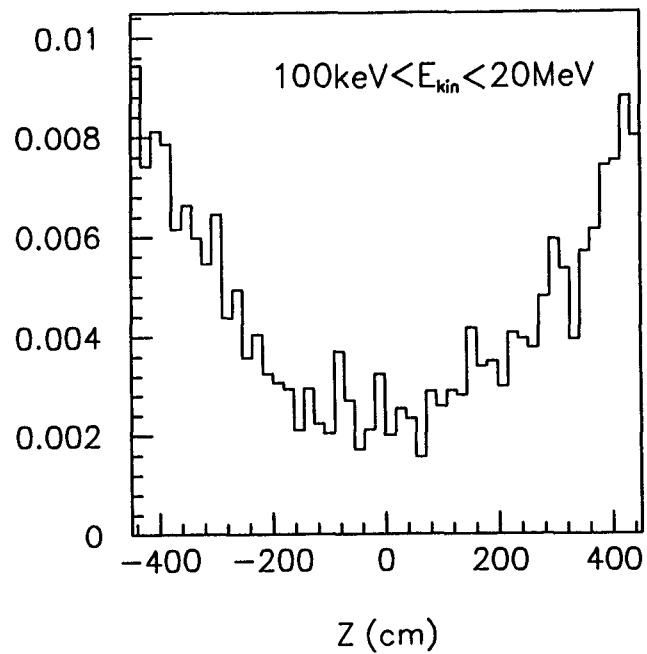
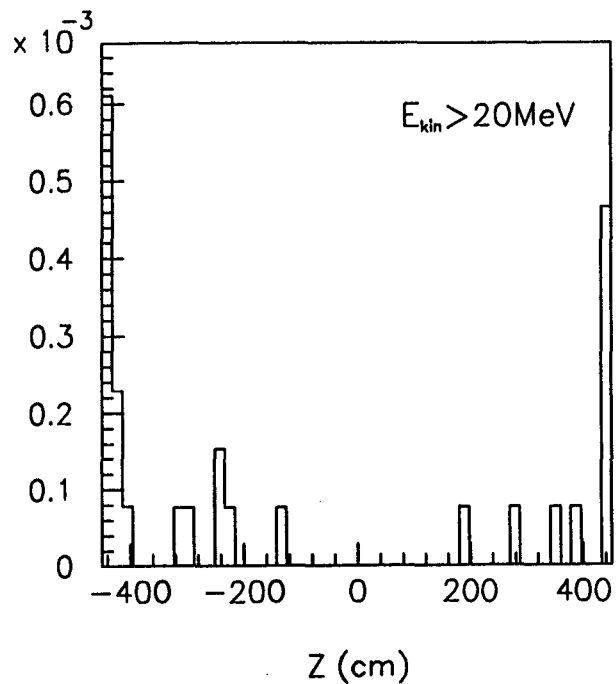


Figure 17: Neutron currents at the outside of the barrel calorimeter phototubes, at $r=463.1$ cm.

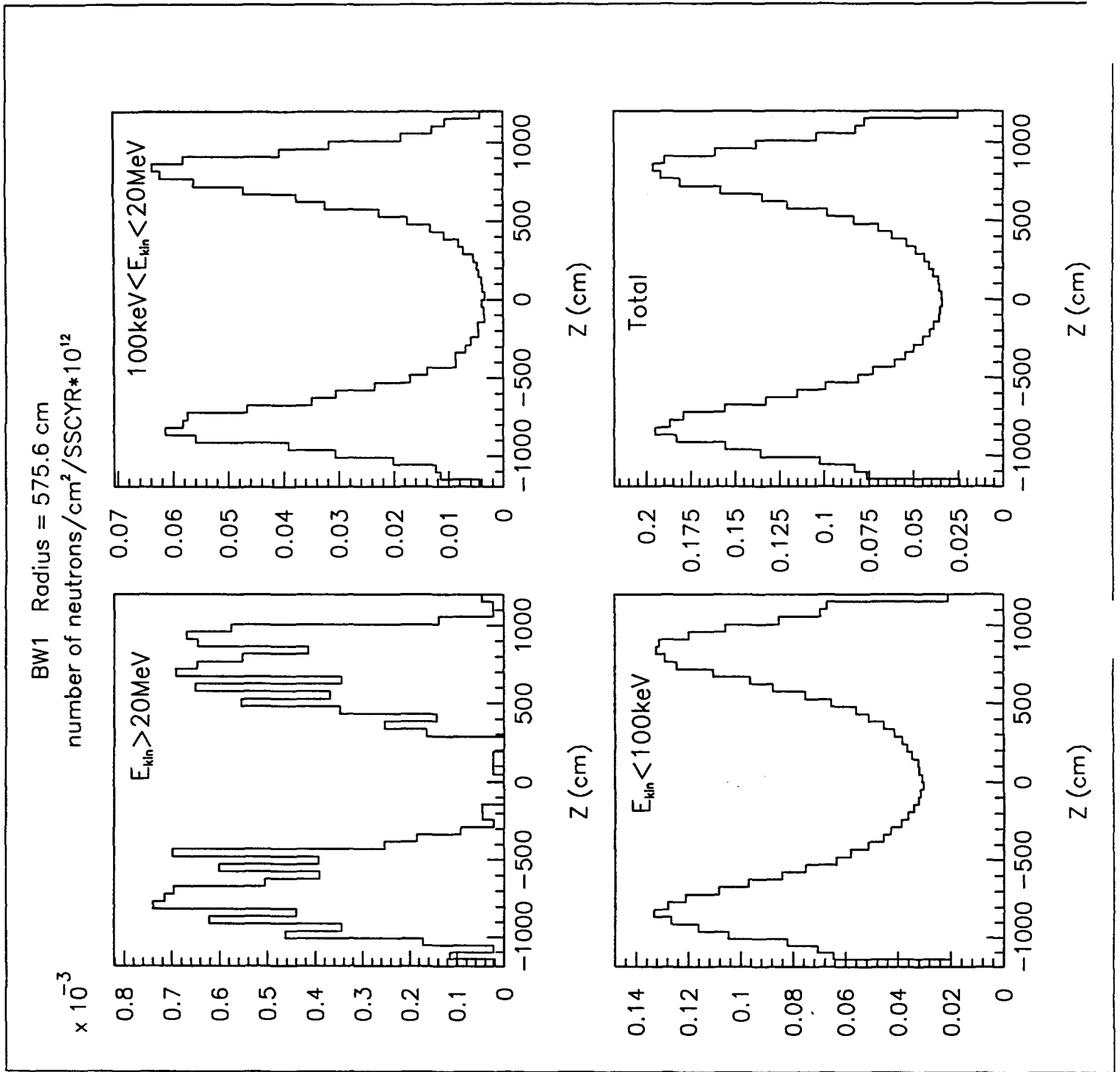


Figure 18: Neutron currents through a cylinder at $r=575.6$ cm, the location of the first planes of the barrel muon chambers (BW1). The muon chambers see albedo neutrons from the forward calorimeter and from the collimator. Those backplash neutrons are attenuated by the forward and barrel toroids.

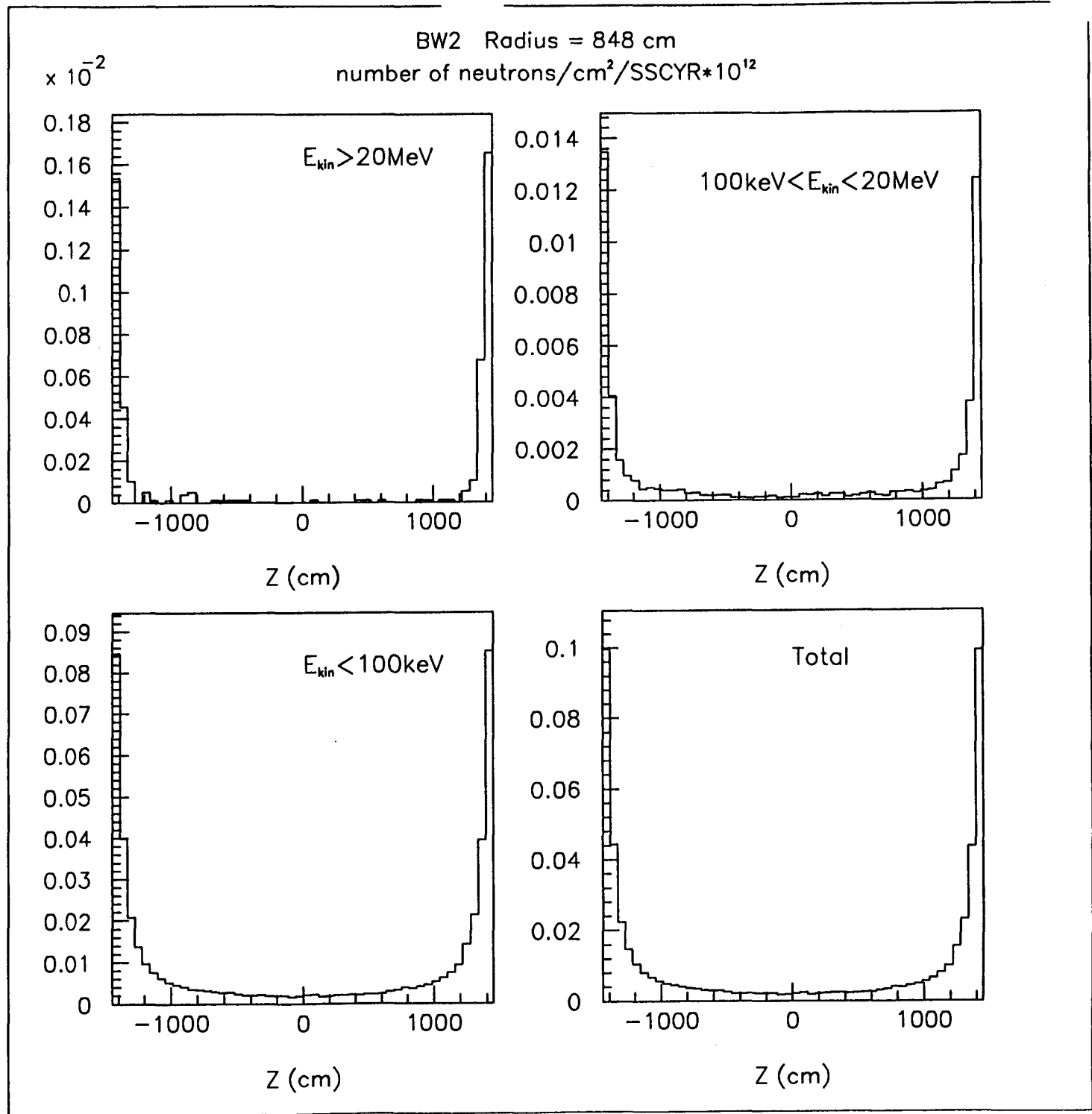


Figure 19: Neutron currents through a cylinder at $r=848$ cm, the location of the second planes of the barrel muon chambers (BW2).

BW3 Radius = 990.1 cm
number of neutrons/cm²/SSCYR*10¹²

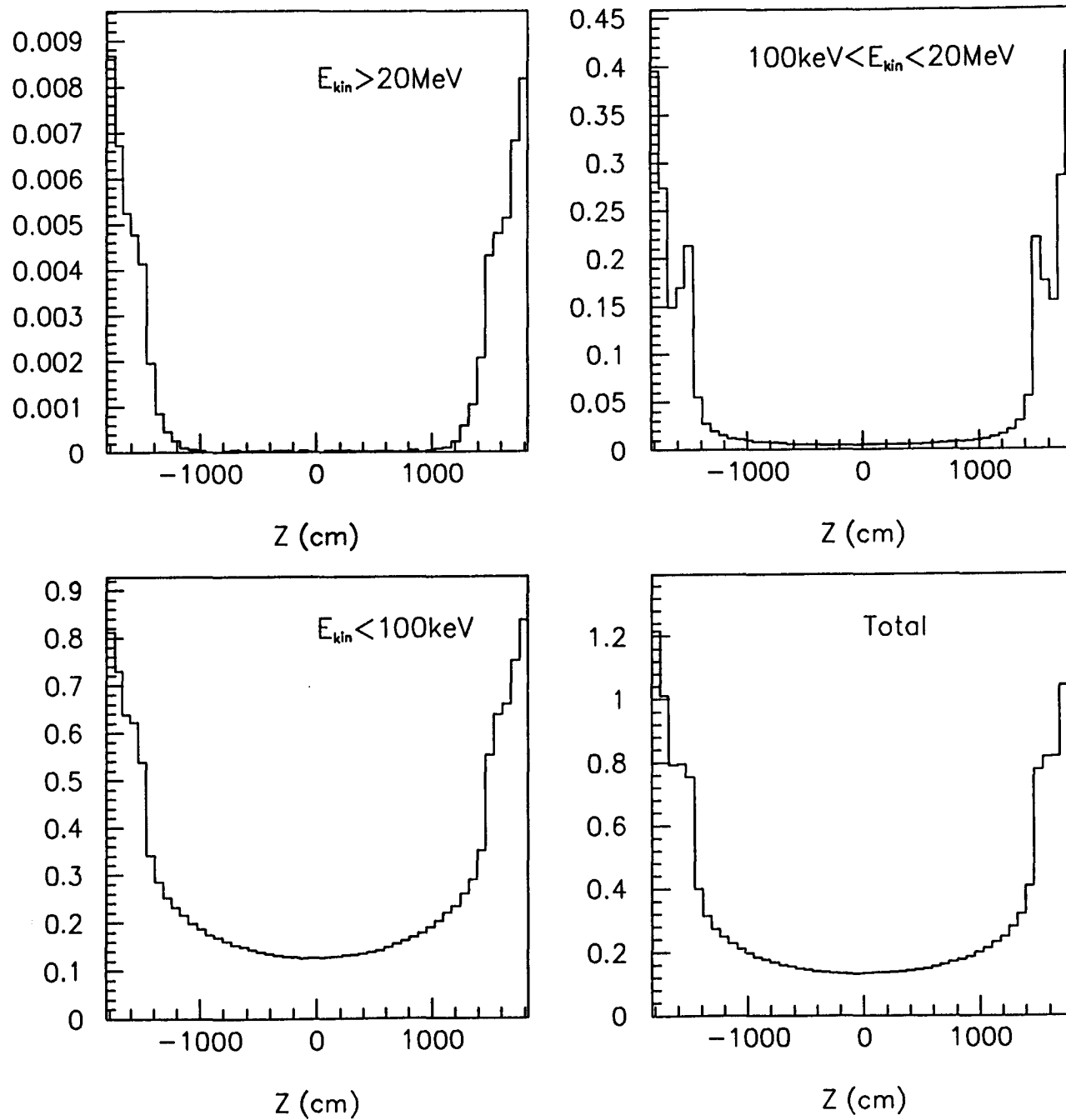


Figure 20: Neutron currents through a cylinder at $r=990.1$ cm, the location of the third planes of the barrel muon chambers (BW3).

FCAL front face Z=1247.6 cm
number of neutrons/cm²/SSCYR*10¹²

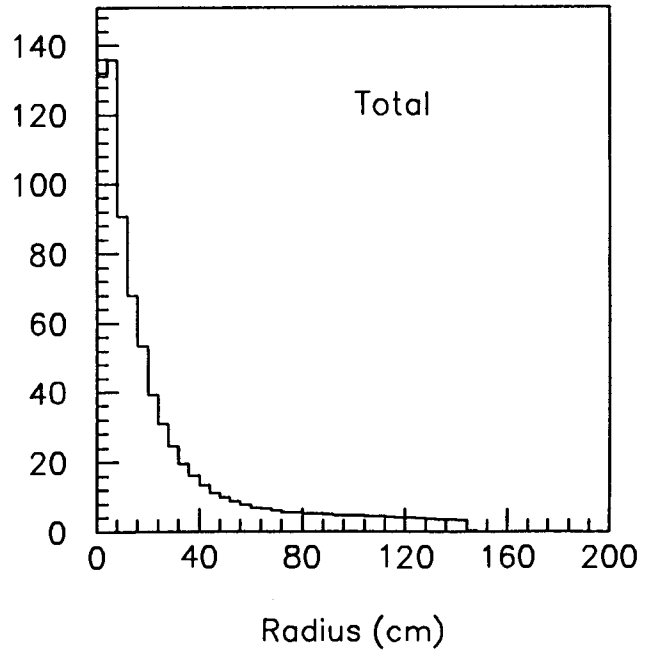
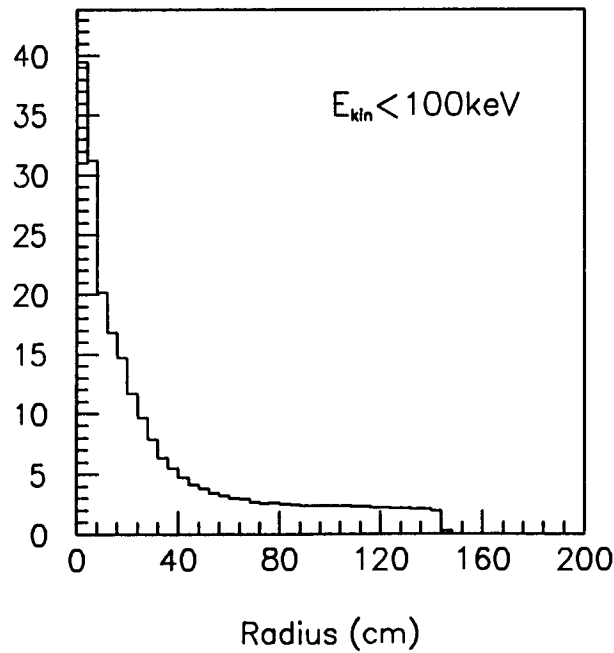
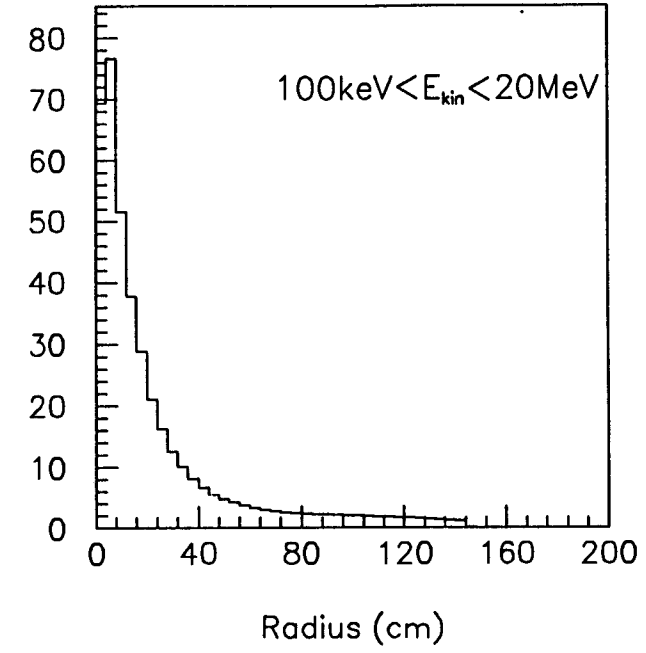
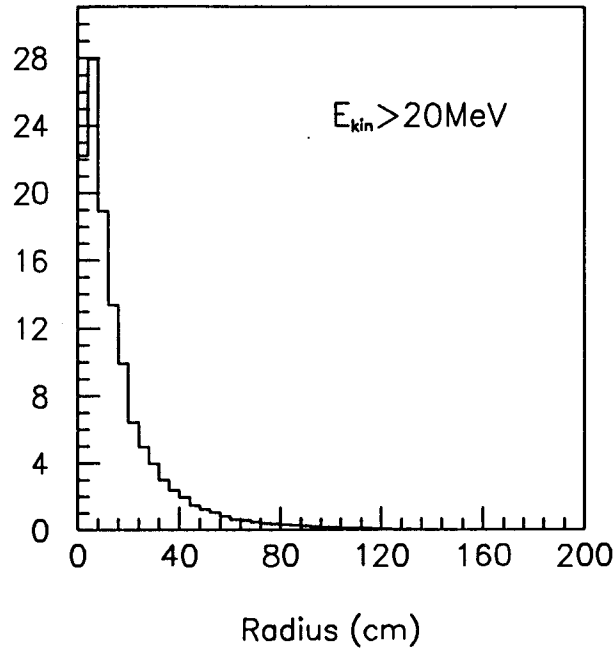


Figure 21: Neutron currents of neutrons moving back toward the detector from the front face of the forward calorimeter, at z=1274.6 cm.

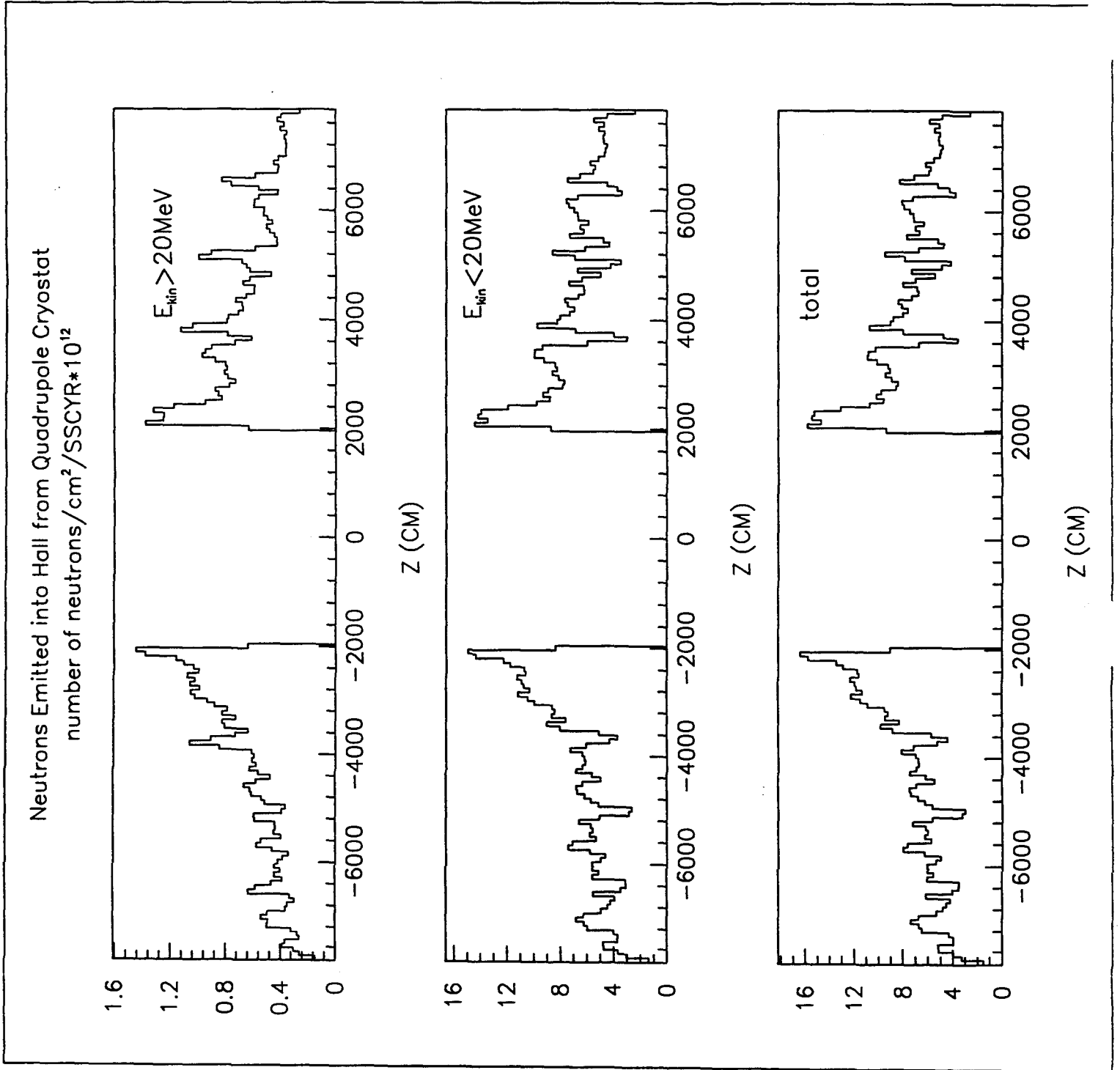


Figure 22: Neutron currents for neutrons emitted into the SDC hall or into the accelerator tunnel from the quadrupole cryostat as a function of z . The peaks in the high energy spectrum and the dips in the low energy spectrum correspond to the drift spaces between the magnets.

WALL AT 55 METERS — TRANSMITTED NEUTRONS

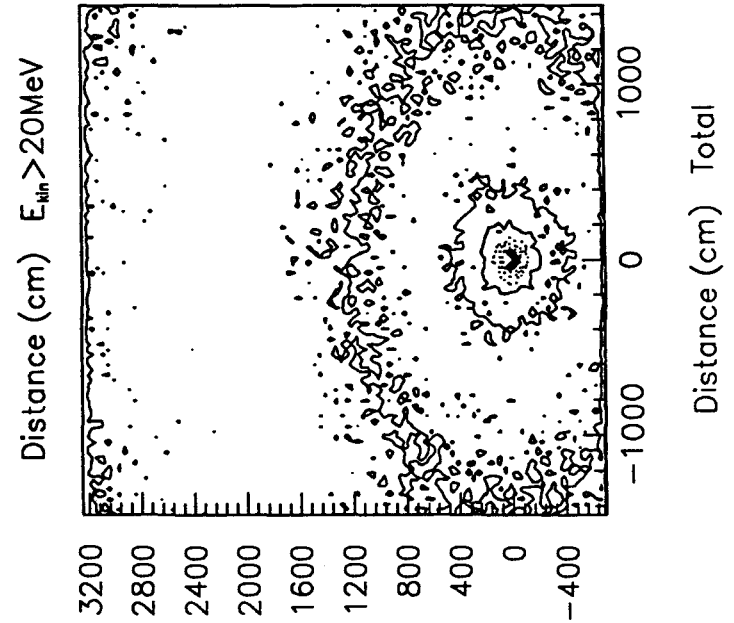
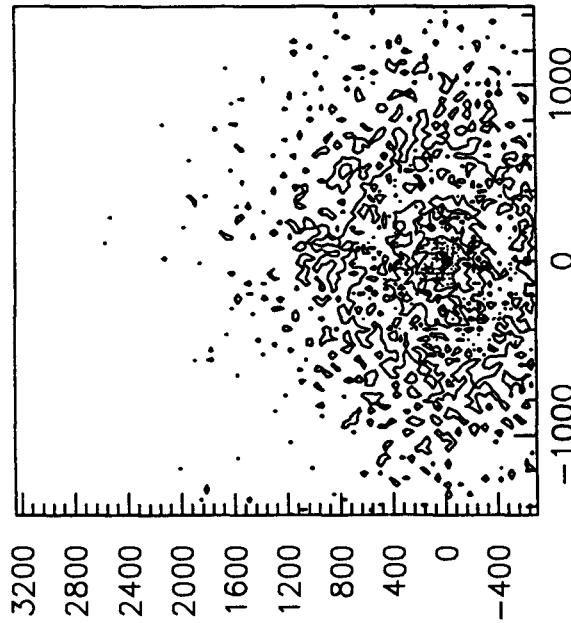
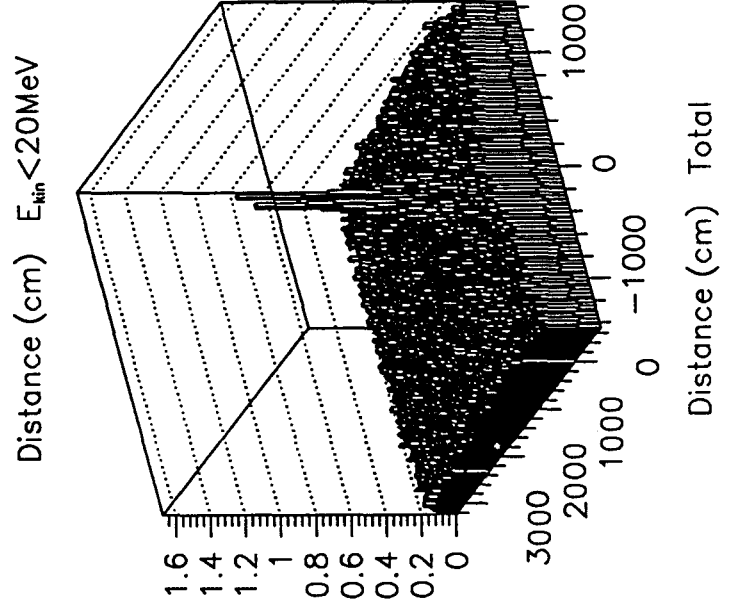
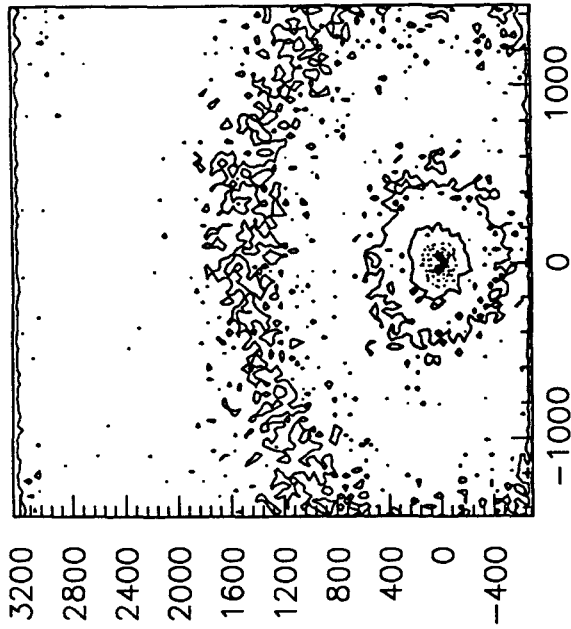


Figure 23: The transmitted neutron currents for the detector hall wall at $z=55 \text{ m}$, as a function of x -position and y -position in cm. These plots show the neutrons transmitted by the wall, that is, neutrons that continue traveling away from the detector.

WALL AT 55 METERS—ALBEDO NEUTRONS

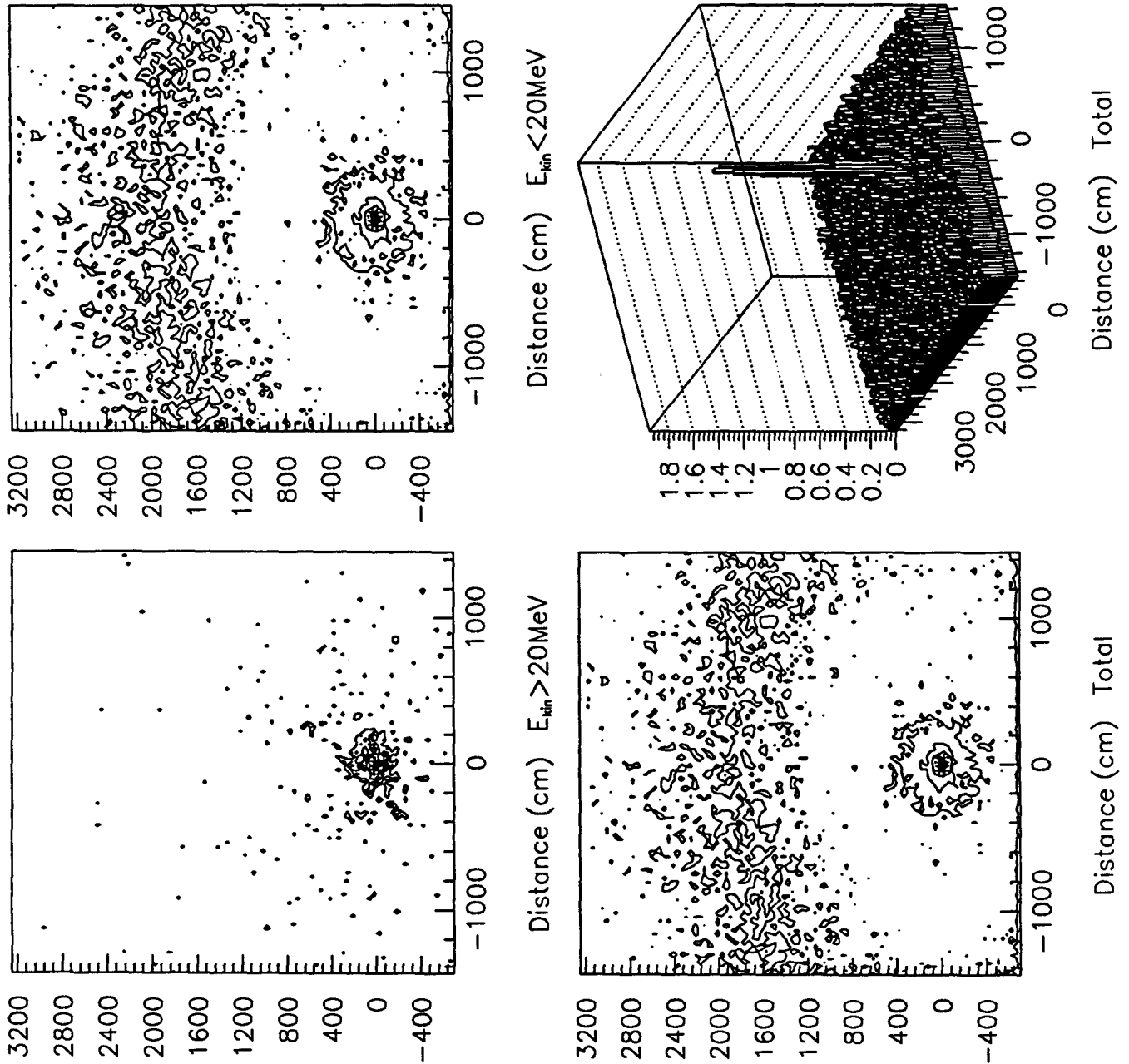


Figure 24. The reflected neutron currents for the detector hall wall at $z=55$ m, as a function of x -position and y -position in cm. These plots show the neutrons reflected by the wall, that is, neutrons that travel toward the detector. Note the rough equality between the currents shown in Figures 23 and 24, which indicates that most of the transmitted neutrons are eventually reflected.